

REFERENCE

FAA-76-22.VII
Report No. FAA-RD-75-173, VII

**AIR TRAFFIC CONTROL EXPERIMENTATION AND EVALUATION
WITH THE NASA ATS-6 SATELLITE**

Volume VII: Aircraft Antenna Evaluation Test

C.J. Kuo
E.H. Schroeder
B.P. Stapleton

Boeing Commercial Airplane Company
PO Box 3707
Seattle WA 98124



**SEPTEMBER 1976
FINAL REPORT**

Document is available to the U.S. public through the
National Technical Information Service,
Springfield, Virginia 22161

Prepared for
U.S. DEPARTMENT OF TRANSPORTATION
Federal Aviation Administration
Systems Research and Development Service
Washington DC 20591

NOTICE

This document is disseminated under the sponsorship of the Department of Transportation in the interest of information exchange. The United States Government assumes no liability for its contents or use thereof.

NOTICE

The United States Government does not endorse products or manufacturers. Trade or manufacturers' names appear herein solely because they are considered essential to the object of this report.

REPORT NO. FAA-RD-75-173,VII

**AIR TRAFFIC CONTROL EXPERIMENTATION AND EVALUATION
WITH THE NASA ATS-6 SATELLITE**

Volume VII: Aircraft Antenna Evaluation Test

ERRATA

Pages 5-3 and 5-5 of this
volume are replaced by the
attached figures.

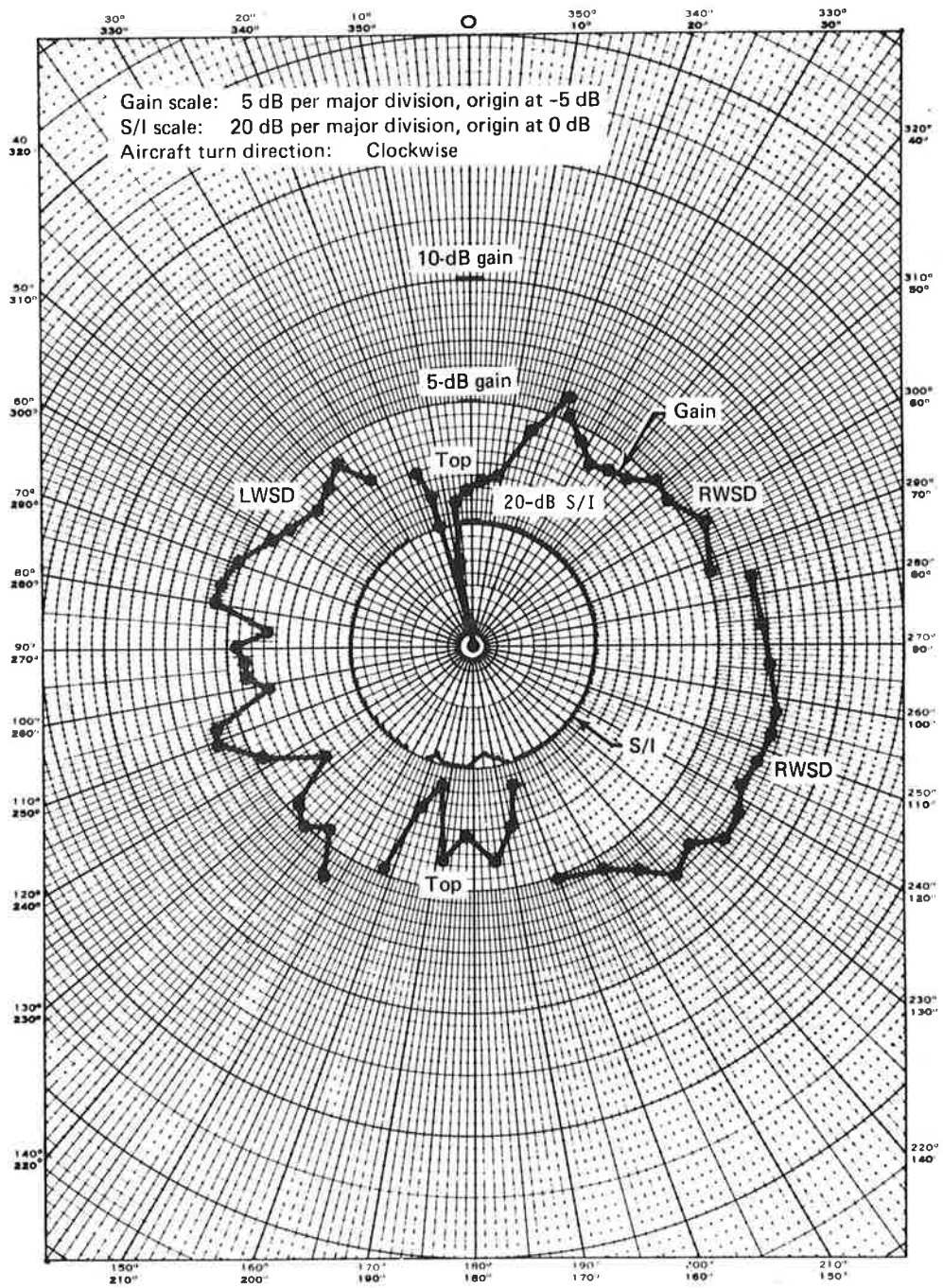


Figure 5-2. Three-Element Slot-Dipole Antenna System Gain and S/I, March 25, 1975, Elevation Angle = 15°

1. Report No. FAA-RD-75-173, VII		2. Government Accession No.		3. Recipient's Catalog No.	
4. Title and Subtitle AIR TRAFFIC CONTROL EXPERIMENTATION AND EVALUATION WITH THE NASA ATS-6 SATELLITE Volume VII: Aircraft Antenna Evaluation Test				5. Report Date September 1976	
				6. Performing Organization Code DOT-TSC-FAA-76-22, VII	
7. Author(s) C.J. Kuo, E.H. Schroeder, B.P. Stapleton				8. Performing Organization Report No. D6-44052	
9. Performing Organization Name and Address Boeing Commercial Airplane Company* P.O. Box 3707 Seattle, WA 98124				10. Work Unit No. FA711/R7106	
				11. Contract or Grant No. DOT-TSC-707-7	
				13. Type of Report and Period Covered Final Report Sep. 1973 to Dec. 1975	
12. Sponsoring Agency Name and Address U.S. Department of Transportation Federal Aviation Administration Systems Research and Development Service Washington, DC 20591				14. Sponsoring Agency Code	
15. Supplementary Notes U.S. Department of Transportation *Under Transportation Systems Center contract to: Kendall Square Cambridge, MA 02142					
16. Abstract <p>Aircraft L-band antennas designed for satellite communication were evaluated using an FAA KC-135 aircraft and the NASA ATS-6 satellite. All tests were performed between September 1974 and April 1975 as one component of the U.S. DOT/FAA aeronautical technology tests. The U.S. DOT/FAA test program was part of the international ATS-6 L-Band Experiment. Three antenna systems were evaluated: (1) a three-element slot-dipole system with antennas mounted on the top and on either side, (2) a microstrip phased array with steerable beam in the roll plane, and (3) a "patch" consisting of a single microstrip element.</p> <p>Antenna performance was evaluated during controlled overocean flight. Data was acquired for a range of satellite elevation angles between 10° and 40°. Two RF receiving channels were used to allow simultaneous reception of data for two antennas. Antenna gain and S/I (the ratio of direct signal to multipath interference) as a function of aircraft/satellite geometry were determined by off-line analysis and presented in the form of plots and tabulations.</p> <p>The report consists of seven volumes: I – Executive Summary; II – Demonstration of Satellite-Supported Communications and Surveillance for Oceanic Air Traffic Control; III – Summary of U.S. Aeronautical Technology Test Program; IV – Data Reduction and Analysis Software; V – Multipath Channel Characterization Test; VI – Modem Evaluation Test; VII – Aircraft Antenna Evaluation Test.</p>					
17. Key Words Aircraft Antennas, L-Band Antennas, Phased Array, Slot Dipole, Quad Helix, ATS-6 Satellite, Antenna Gain, S/I, C/N ₀ , Noise Figure, Noise Temperature, Insertion Loss				18. Distribution Statement Document is available to the U.S. public through the National Technical Information Service, Springfield, Virginia 22161	
19. Security Classif. (of this report) Unclassified		20. Security Classif. (of this page) Unclassified		21. No. of Pages 84	22. Price

**AIR TRAFFIC CONTROL EXPERIMENTATION AND
EVALUATION WITH THE NASA ATS-6 SATELLITE**

FINAL REPORT

This report consists of the following volumes.



**Volume I
Executive Summary**



**Volume II
Demonstration of Satellite-Supported Communications
and Surveillance for Oceanic Air Traffic Control**



**Volume III
Summary of U.S. Aeronautical Technology
Test Program**



**Volume IV
Data Reduction and Analysis Software**



**Volume V
Multipath Channel Characterization Test**



**Volume VI
Modem Evaluation Test**



**Volume VII
Aircraft Antenna Evaluation Test**

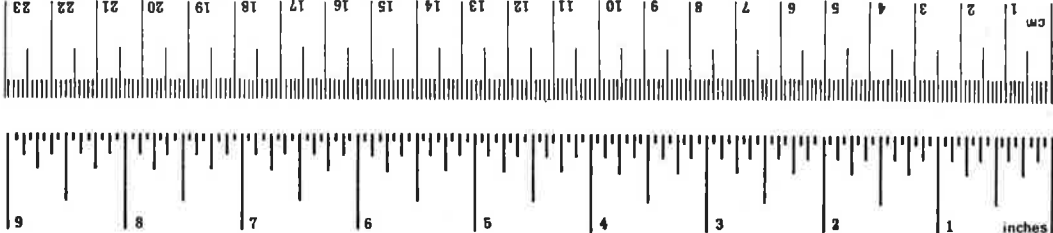
PREFACE

The U.S. Department of Transportation (DOT) aeronautical test program entitled "Air Traffic Control Experimentation and Evaluation with the NASA ATS-6 Satellite" was part of the Integrated ATS-6 L-Band Experiment. The overall ATS-6 L-band experiment was coordinated by the NASA/Goddard Space Flight Center (GSFC) and was international in scope. The following agencies were participants in the experiment: NASA/Goddard Space Flight Center; DOT/Federal Aviation Administration; DOT/Transportation Systems Center; DOT/U.S. Coast Guard; DOC/Maritime Administration; European Space Agency (ESA); and the Canadian Ministry of Transport and Department of Communications. Each participant performed tests in one or more of three categories: aeronautical, maritime safety, and maritime fleet operations. All tests were conducted in accordance with an overall integrated test plan coordinated by NASA/GSFC.

The U.S. DOT Aeronautical test program was under the direction and sponsorship of the Federal Aviation Administration, Systems Research and Development Service (SRDS), Satellite Branch, with the DOT/TSC conducting the technology tests and the FAA/NAFEC conducting the ATC demonstration tests. The technology tests included multipath channel characterization, modem evaluation, and aircraft antenna evaluation. Results of these tests are presented in Volumes III through VII, and the results of the ATC demonstration tests are presented in Volume II. The DOT/TSC test program was supported by the Boeing Commercial Airplane Company under contract DOT-TSC-707. Mr. R. G. Bland was the TSC Project Engineer and Contract Technical Monitor.

METRIC CONVERSION FACTORS

Approximate Conversions to Metric Measures			Approximate Conversions from Metric Measures					
Symbol	When You Know	Multiply by	To Find	Symbol	When You Know	Multiply by	To Find	Symbol
LENGTH								
in	inches	2.54	centimeters	cm	millimeters	0.04	inches	in
ft	feet	30	centimeters	cm	centimeters	0.4	inches	in
yd	yards	0.9	meters	m	meters	3.3	feet	ft
mi	miles	1.6	kilometers	km	kilometers	1.1	yards	yd
						0.6	miles	mi
AREA								
in ²	square inches	6.5	square centimeters	cm ²	square centimeters	0.16	square inches	in ²
ft ²	square feet	0.09	square meters	m ²	square meters	1.2	square yards	yd ²
yd ²	square yards	0.8	square meters	m ²	square kilometers	0.4	square miles	mi ²
mi ²	square miles	2.6	square kilometers	km ²	hectares (10,000 m ²)	2.5	acres	ac
	acres	0.4	hectares	ha				
MASS (weight)								
oz	ounces	28	grams	g	grams	0.035	ounces	oz
lb	pounds	0.45	kilograms	kg	kilograms	2.2	pounds	lb
	short tons (2000 lb)	0.9	tonnes	t	tonnes (1000 kg)	1.1	short tons	st
VOLUME								
tsp	teaspoons	5	milliliters	ml	milliliters	0.03	fluid ounces	fl oz
Tbsp	tablespoons	15	milliliters	ml	liters	2.1	pints	pt
fl oz	fluid ounces	30	milliliters	ml	liters	1.06	quarts	qt
c	cups	0.24	liters	l	liters	0.26	gallons	gal
pt	pints	0.47	liters	l	cubic meters	35	cubic feet	ft ³
qt	quarts	0.96	liters	l	cubic meters	1.3	cubic yards	yd ³
gal	gallons	3.8	liters	l				
ft ³	cubic feet	0.03	cubic meters	m ³				
yd ³	cubic yards	0.76	cubic meters	m ³				
TEMPERATURE (exact)								
°F	Fahrenheit temperature	5/9 (after subtracting 32)	Celsius temperature	°C	°C	9/5 (then add 32)	Fahrenheit temperature	°F



*1 in = 2.54 (exactly). For other exact conversions and more detailed tables, see NBS Misc. Publ. 236, Units of Weights and Measures, Price \$2.25, SD Catalog No. C13.10.286.

CONTENTS

<u>Section</u>		<u>Page</u>
1.	INTRODUCTION	1-1
1.1	DOT/TSC Aeronautical Technology Tests.....	1-1
1.2	DOT/FAA Air Traffic Control Demonstration Tests.....	1-1
2.	SUMMARY OF RESULTS AND CONCLUSIONS	2-1
2.1	Three-Element Slot-Dipole System	2-1
2.2	Phased-Array Antenna.....	2-2
2.3	Patch Antenna.....	2-3
3.	ANTENNA EVALUATION TEST DESCRIPTION.....	3-1
3.1	Test Objectives	3-1
3.2	Test Implementation.....	3-1
3.2.1	KC-135 L-Band Antennas	3-1
3.2.2	Satellite Link Configuration	3-4
3.2.3	KC-135 Terminal Configuration	3-6
3.3	Flight Test and Planning Procedures	3-11
3.3.1	Test Geometries and Scenarios	3-11
3.3.2	Real-Time Calibration Measurements	3-13
3.4	Antenna Test Data Acquisition Summary	3-15
4.	DATA ANALYSIS DESCRIPTION.....	4-1
4.1	Data Analysis Procedures	4-1
4.1.1	Bearing and Elevation Angles Computation.....	4-1
4.1.2	C/N ₀ and S/I Determination.....	4-3
4.1.3	Antenna Gain Calculation.....	4-3
4.2	Antenna Data Presentation	4-7
5.	THREE-ELEMENT SLOT-DIPOLE ANTENNA SYSTEM RESULTS.....	5-1
5.1	Experimental Gain and S/I Data	5-1
5.2	Gain and S/I Determined from Antenna Range Measurements	5-12
5.3	Discussion of Results and Conclusions	5-15

CONTENTS (Concluded)

Section	Page
6. PHASED-ARRAY ANTENNA TEST RESULTS.....	6-1
6.1 Experimental Gain and S/I Data	6-1
6.2 Antenna Range Pattern Measurements	6-9
7. PATCH ANTENNA TEST RESULTS.....	7-1
REFERENCES	R-1
APPENDIX— Prediction of S/I from Antenna Range Data for Slot-Dipole Antennas	A-1

ILLUSTRATIONS

Figure	Page
3-1 KC-135 Antenna Locations.....	3-2
3-2 Link Configuration for DOT ATS-6 L-Band ATC Experimentation and Evaluation Tests	3-5
3-3 Simplified KC-135 Terminal for Antenna Evaluation Test	3-7
3-4 Carrier Detector Unit	3-9
3-5 Antenna Evaluation Test Geometry	3-12
4-1 Aircraft Heading Pitch and Roll Data, October 29, 1974	4-2
5-1 Three-Element Slot-Dipole Antenna System Gain and S/I, April 1, 1975, Elevation Angle = 15°.....	5-2
5-2 Three-Element Slot-Dipole Antenna System Gain and S/I, March 25, 1975, Elevation Angle = 15°.....	5-3
5-3 Three-Element Slot-Dipole Antenna System Gain and S/I, November 21, 1974, Elevation Angle = 19°.....	5-4
5-4 Slot-Dipole-System Composite Gain at 20° Elevation.....	5-5
5-5 Three-Element Slot-Dipole Antenna System Gain and S/I, October 24, 1974, Elevation Angle = 19°.....	5-6
5-6 Three-Element Slot-Dipole Antenna System Gain and S/I, October 29, 1974, Elevation Angle = 16°.....	5-7

ILLUSTRATIONS (Concluded)

<u>Figure</u>		<u>Page</u>
5-7	Three-Element Slot-Dipole Antenna System Gain and S/I, September 24, 1974, Elevation Angle = 28°	5-8
5-8	Three-Element Slot-Dipole Antenna System Gain and S/I, October 23, 1974, Elevation Angle = 25°	5-9
5-9	Wing-Root Slot-Dipole Antenna Range Gain at Elevation Angles of 10° and 20°	5-13
5-10	Wing-Root Slot-Dipole Antenna Range Gain at Elevation Angles of 30° and 40°	5-14
5-11	Computed S/I for Wing-Root Slot-Dipole Antenna	5-16
6-1	Phased-Array Gain Data for "Straight-Line" Tests	6-3
6-2	Phased-Array Antenna Gain and S/I, September 24, 1974, Elevation Angle = 28°	6-4
6-3	Phased-Array Antenna Gain and S/I, October 29, 1974, Elevation Angle = 16°	6-5
6-4	Phased-Array Antenna Gain and S/I, October 24, 1974, Elevation Angle = 19°	6-6
6-5	Phased-Array Antenna Gain and S/I, November 21, 1974, Elevation Angle = 19°	6-7
6-6	Phased-Array Antenna Gain and S/I, October 23, 1974, Elevation Angle = 25°	6-8
6-7	Phased-Array Roll-Plane Directivity Determined From Antenna Range Measurements, Beam Position 2	6-11
7-1	Patch Antenna Gain and S/I, October 23, 1974, Elevation Angle = 25°	7-2
7-2	Patch Antenna Gain and S/I, November 21, 1974, Elevation Angle = 19°	7-3
7-3	Patch Antenna Gain and S/I, October 29, 1974, Elevation Angle = 16°	7-4
7-4	Patch Antenna Gain and S/I, October 24, 1974, Elevation Angle = 19°	7-6

TABLES

<u>Table</u>		<u>Page</u>
3-1	ANTENNA EVALUATION DATA ACQUISITION SUMMARY	3-16
4-1	RECEIVING CHANNEL CHARACTERIZATION FOR ANTENNA EVALUATION TEST	4-5
4-2	ANTENNA EVALUATION TEST DATA TABULATION EXAMPLE	4-8
5-1	SLOT-DIPOLE-ANTENNA CIRCULAR FLIGHT SUMMARY	5-1
5-2	RWSD ANTENNA GAIN DATA, JANUARY 21, 1975, ELEVATION ANGLE = 40°	5-11
5-3	COMPARISON OF SPECULAR-POINT AND SURFACE INTEGRATION MODEL PREDICTION OF S/I FOR SLOT-DIPOLE ANTENNA	5-15
6-1	PHASED-ARRAY GAIN DATA FOR LINEAR FLIGHTPATHS	6-2
6-2	PHASED-ARRAY CIRCULAR FLIGHT SUMMARY	6-10
7-1	PATCH ANTENNA CIRCULAR FLIGHT SUMMARY	7-1
7-2	PATCH ANTENNA GAIN DATA, JANUARY 21, 1975, ELEVATION ANGLE = 40°	7-1

SYMBOLS AND ABBREVIATIONS

AGC	automatic gain control
ATS-6	Applications Technology Satellite 6 (NASA)
bpi	bits per inch
BER	bit-error rate
cw	continuous wave
CAD	coherent amplitude detection
C/N_o	carrier-to-noise power density ratio
CONUS	Continental United States
dB	decibel
DOT	Department of Transportation
ENR	excess noise ratio
FDM	frequency division multiplex
FFT	fast Fourier transform
FMP	forward multipath (antenna)
GMT	Greenwich mean time
IF	intermediate frequency
IL	insertion loss
IRIG	Inter-Range Instrumentation Group
LHC	left-hand circular
NAFEC	National Aviation Facilities Experimental Center
NF_{op}	system operating noise figure
PAT	patch (antenna)
PHA	phased-array (antenna)
PLACE	position location and communication equipment
PN	pseudo-noise
QH	quad-helix (antenna)
RF	radiofrequency
RHC	right-hand circular
RX	receiver
SACP	satellite aeronautical channel prober
SDP	slot-dipole (antenna)
S/I	ratio of direct signal to multipath interference
SMP	side-mounted multipath (antenna)
TDPC	Test Data Processing Center

SYMBOLS AND ABBREVIATIONS (Concluded)

TOP/LWSD/RWSD	top, left-wing, and right-wing slot-dipole (antenna)
TSC	Transportation Systems Center
TX	transmitter
VCXO	voltage-controlled crystal oscillator.

1. INTRODUCTION

The U.S. aeronautical technology tests were conducted by the U.S. Department of Transportation/Transportation Systems Center (DOT/TSC) as part of the Integrated L-Band Experiment (ref. 1-1). The overall objective of these tests is to provide data for the evaluation of advanced system concepts and hardware applicable to the design of future satellite-based air traffic control systems.

1.1 DOT/TSC AERONAUTICAL TECHNOLOGY TESTS

Three types of aeronautical technology tests were conducted by DOT/TSC:

- a. *Multipath Channel Characterization:* Pseudo-noise (PN) code modulated signals were transmitted from the KC-135 using several different antennas and various polarizations. After relay by ATS-6, the signals were received at Rosman, processed by the SACP equipment, recorded, and later analyzed to obtain a characterization of the multipath channel. The multipath tests are described in volume V.
- b. *Modem Evaluation:* Several voice, digital data, ranging, and hybrid voice/data modems were tested using signals transmitted from Rosman through ATS-6 to the aircraft. Modem demodulator outputs were recorded onboard the aircraft and analyzed to determine performance for various carrier-to-noise density (C/N_0) and signal-to-multipath interference (S/I) ratios. The modem evaluation tests are described in volume VI.
- c. *Antenna Evaluation:* A cw signal radiated by Rosman through ATS-6 was received by the various aircraft antennas under test. Data was recorded and analyzed to evaluate antenna gain and multipath rejection as a function of geometry.

This volume describes the antenna evaluation tests. Section 2 summarizes the results and conclusions. Sections 3 and 4 give a general description of the tests and data analysis procedures. Sections 5 through 7 present experimental data for the TOP/LWSD/RWSD slot dipole, phased-array, and patch antenna systems.

1.2 DOT/FAA AIR TRAFFIC CONTROL DEMONSTRATION TESTS

Demonstration tests were conducted by the Federal Aviation Administration as part of the overall U.S. Department of Transportation L-band aeronautical test program. The tests evaluated voice and digital data communications (including full duplex operations) over L-band aeronautical satellite links in an operational type environment described in volume II of this report.

2. SUMMARY OF RESULTS AND CONCLUSIONS

2.1 THREE-ELEMENT SLOT-DIPOLE SYSTEM

The three-element slot-dipole antenna system consists of three flush-mounted antennas located on either side in the upper wing-body fairing area and on the top centerline. One antenna was selected at a given time. The system was designed to provide gain of at least 4 dB over at least 90% of the upper hemisphere while simultaneously achieving a predicted multipath rejection ratio in excess of 10 dB.

Performance data for this antenna system was acquired experimentally over a range of satellite elevation angles between 10° and 40° . At elevation angles above 20° , the experimentally measured antenna gain was in excess of 4 dB at essentially all azimuthal angles except in the forward direction for the TOP antenna. In the forward direction ($\pm 20^{\circ}$ from the nose), the TOP antenna gain was 3.5 dB for an elevation angle of 20° . The peak gain measured for the side-mounted antennas was approximately 10 dB. At the higher elevation angles, the experimentally measured gain frequently exceeded the gain values determined from scale-model antenna range data by about 2 dB. At elevation angles below 20° , the experimental gain measurements were quite sensitive to aircraft motions affecting the aircraft/satellite geometry but were in general agreement with range data. Although experimental scatter was observed in the measured gain data, there was no evidence of significant pattern holes or coverage deficiencies at any of the geometries tested. The experimental data suggests that the slot dipoles may be somewhat more directional in the roll plane than indicated by the antenna range scale-model measurements, but the experimental data scatter and the relatively small amount of data available preclude drawing firm conclusions on this point.

Specific items with potential for causing the experimentally measured gains to exceed those determined from antenna range measurements have been investigated but have not been positively isolated as contributors. Two possibilities considered (discussed further in sec. 5.3) are described below.

- a. The overall RF insertion losses between the antenna and the preamplifier have an uncertainty (in all cases less than 1.0 dB) that translates directly into a corresponding uncertainty in the calculated antenna gain. Calculated gains for the RWSD and LWSD could therefore be too large by 0.5 to 1.0 dB due to this contribution.
- b. The antenna gain values calculated from the experimental data would contain a systematic error making their values too high if the actual in-flight gain achieved with the quad-helix reference antenna was less than the 15.5-dB value determined from full-scale measurements on the antenna range. It is believed that this systematic error is less than 0.5 dB.

The experimentally measured gain of the TOP antenna was usually observed to be less in the forward than in the aft direction, indicating that aircraft pitch angle may be influencing performance. This suggests that a more forward location of the TOP antenna might result in improved over-the-nose performance at low elevation angles.

The experimental data showed conclusively that very good multipath rejection was achieved by the three-element slot-dipole antenna system at all geometries tested. The S/I was usually greater than 20 dB, with occasional dips into the 15- to 20-dB range, and with a few more severe drops in the vicinity of the nose for the top-mounted antenna. This performance is in general agreement with the predicted S/I values based on antenna range measurements.

The rather large S/I values observed are consistent with results for Type I digital data modem tests, where the bit-error-rate (BER) performance curves have the same character as predicted for a purely additive noise environment without multipath interference.

2.2 PHASED-ARRAY ANTENNA

The phased array is a low-profile microstrip antenna consisting of a 1- by 8-array attached to the outer fuselage at station 420 on the right side to give broad lateral coverage. The antenna elements are phased electronically to provide beam steering in elevation in nine increments of about 10° each. The peak gain derived from full-scale antenna range measurements is approximately 12.0 dB.

Experimental antenna performance data was acquired over a range of elevation angles between 10° and 40° . The circular and straight-line flight test data show that the phased array, as mounted on the KC-135, provided a peak gain of 11 to 12 dB approximately broadside at an elevation angle of 40° . This measured value agrees well with the full-scale antenna range peak gain value. At an elevation angle of 40° , the 3-dB azimuthal beamwidth was approximately 100° , providing coverage between 50° and 150° from the nose. From the small amount of data available at elevation angles of 10° , the experimentally measured maximum achievable gain was between 9.0 and 9.5 dB and the 3-dB azimuthal beamwidth was approximately 50° . At azimuthal angles beyond the above useful coverage region, the gain dropped rapidly to low or negative values. No attempt was made to measure side-lobe levels experimentally.

The antenna exhibited consistently good multipath rejection, with the measured S/I being in excess of 20 dB within the useful coverage region.

2.3 PATCH ANTENNA

The patch antenna is a low-profile microstrip antenna attached to the outer fuselage near the top centerline at station 270. It was designed and mounted to give broad coverage, primarily in a forward direction, and was intended to serve as a forward "fill-in" antenna to augment coverage provided by other side-mounted, low-gain antennas that might be used.

Experimental performance data was acquired over a range of satellite elevation angles between 10° and 40° . Results show that the patch antenna had a peak gain of approximately 4 dB forward over the nose at elevation angles above 15° and a minimum S/I of 13 dB. The gain gradually decreased as the satellite bearing angle changed toward the broadside and aft directions or as the satellite elevation angle reduced toward the horizon. Gain in the broadside and aft-of-broadside directions was about 0 dB at an elevation angle of 16° , increasing to about 2.5 dB at 25° .

3. ANTENNA EVALUATION TEST DESCRIPTION

This section provides a general description of the antenna evaluation test objectives, implementations, and test scenarios.

3.1 TEST OBJECTIVES

The antenna evaluation test quantitatively evaluated the in-flight performance of candidate aircraft antennas for aeronautical L-band satellite applications. The antenna performance figures of merit of major interest are the gain (which directly determines achievable C/N_0) and the ratio of received signal to multipath interference (S/I).

The specific test objective was to acquire and analyze data to determine gain and S/I over a range of satellite elevation and relative bearing angles for the selectable three-element slot-dipole system, phased-array, and patch antennas.

3.2 TEST IMPLEMENTATION

3.2.1 KC-135 L-Band Antennas

The approximate locations of the L-band antennas installed on the KC-135 test aircraft are shown in figure 3-1. The principal antennas tested during the antenna evaluation tests were (1) the three-element TOP/LWSD/RWSD slot-dipole system, (2) the phased array, and (3) the patch antenna. Major features of the aircraft L-band antennas are summarized below. Unless otherwise noted, polarization is right-hand circular (RHC).

- a. *Three-Element (TOP/LWSD/RWSD) Slot-Dipole Antenna System:* This system consists of three flush-mounted slot-dipole antennas, one of which is selected manually at a given time. The objective of the system is to provide a gain of at least 4 dB over at least 90% of the upper hemisphere while simultaneously achieving a predicted multipath rejection ratio¹ in excess

¹Predicted multipath rejection ratios referred to are calculated using the specular point model and analysis of the appendix. The actual multipath rejection ratios achieved are dependent upon the sea-surface roughness characteristics and will generally exceed the value computed from the above model. More discussion is given in section 5.2 and the appendix.

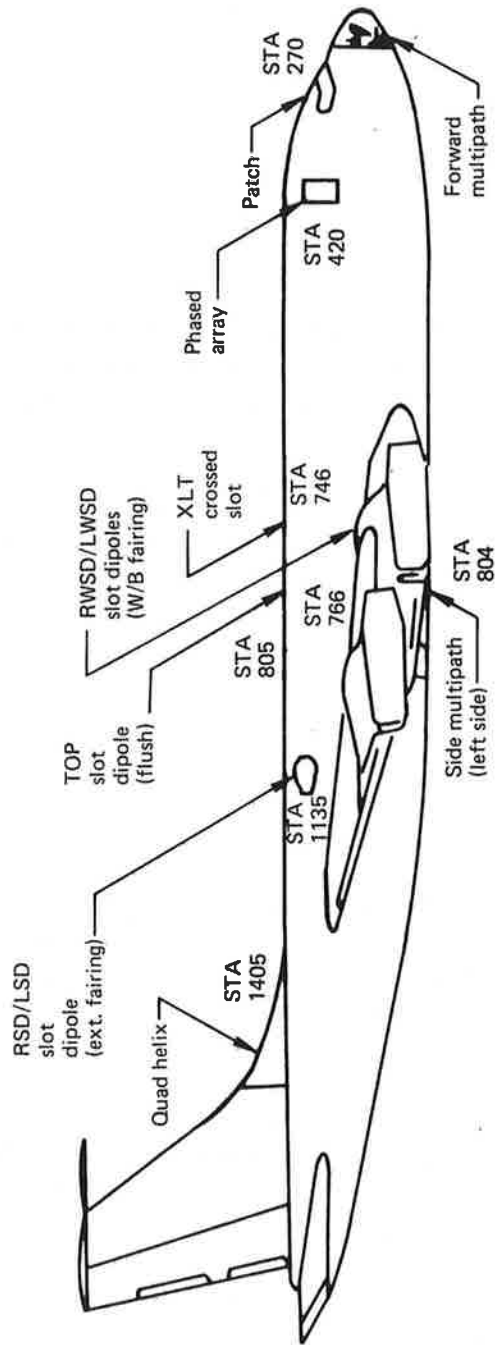


Figure 3-1. KC-135 Antenna Locations

of 10 dB. Side coverage is provided by the left (LWSD) and right (RWSD) side antennas mounted in the upper wing/body (wing-root) fairing areas at station 766. This location was chosen because of the excellent multipath rejection due to the shielding effect of the wing. High elevation angle and fore/aft coverage are provided by a third antenna (TOP) mounted near the top centerline at station 805.

- b. *Phased-Array (PHA) Antenna:* This is a low-profile 1- by 8-array microstrip antenna attached to the outer fuselage on the right side of the aircraft at station 420, 41° down from the top centerline. The antenna elements were arrayed vertically and were phased electronically to provide electronic beam steering in elevation in nine increments of about 10° each. In azimuth, the beamwidth was designed to be about 120° and had fixed pointing approximately broadside.
- c. *Patch (PAT) Antenna:* This antenna was also a low-profile microstrip antenna attached to the outer fuselage near the top centerline at station 270. The mounting location was chosen as nearly optimum for providing forward “fill-in” coverage for the two-element (RSD/LSD) antennas in the event they were used.

In addition to the above antennas that were evaluated, two other antenna systems were used during the antenna evaluation tests:

- a. *Quad-Helix (QH) Antenna:* The quad helix has a conical beam shape approximately 19° in width at the 3-dB points. The antenna is mechanically steerable to provide coverage throughout the forward and broadside regions of the upper hemisphere. At the beam peak, the gain for RHC polarization is 15.5 dB. This antenna was used as the “reference-gain” antenna for determining the gain of other antennas under test.
- b. *Right/Left Slot-Dipole (RSD/LSD) Antennas:* These two antennas were mounted on each side of the fuselage at station 1135 approximately 35° down from the top centerline. Due to the more favorable location of the LWSD/RWSD/TOP slot dipoles, the RSD/LSD antennas were used only as backups in the event of LWSD or RWSD antenna failure and for transmission and reception of auxiliary test coordination communication signals. Antenna evaluation test data was not acquired with these antennas. Performance data for these antennas is available in reference 3-1.

Other L-band antennas installed but not used for antenna evaluation tests include the forward multipath antenna, the side-mounted multipath antenna, and the crossed-slot orthogonal-mode cavity antenna. A brief description of these antennas is included for completeness.

- a. *Forward Multipath (FMP) Antenna:* Gain is approximately 6 dB and polarization is selectable between right-hand circular (RHC), left-hand circular (LHC), and dual linear (the horizontal and vertical polarization ports are simultaneously accessible on separate transmission lines). It is mechanically steerable downward from the horizon in elevation and to both right and left of the aircraft nose in azimuth.
- b. *Side-Mounted Multipath (SMP) Antenna:* This antenna, located below the left wing at station 804 and waterline 150, has a fixed beam that points approximately 15° below the horizon and 10° aft of broadside. Gain is about 13 dB and polarization is selectable between dual linear, RHC, or LHC. This antenna was used to receive the ocean-reflected multipath signals for Type II modem evaluation tests. Reception is maximized for flights approximately broadside to the satellite direction at elevation angles near 15°. Reception of the direct path signal is held to an acceptable low level by the shielding effect of the wing under which the antenna is installed.
- c. *Cross-Slot (XLT) Antenna:* Also referred to as an orthogonal-mode cavity, this antenna was installed at station 746 near the top centerline specifically for acquisition of CONUS multipath data during the February 1975 tests.

The TOP/LWSD/RWSD slot dipoles were furnished and installed by Boeing specifically for this test program.² The phased array and patch were furnished and installed by Ball Brothers Research Corp. Detailed description and evaluation of these antennas may be found in reference 3-2 to 3-4. The side multipath, RSD/LSD slot dipoles, and quad helix were developed and installed by Boeing for the earlier FAA ATS-5 tests (ref. 3-1). The crossed-slot antenna was furnished by Boeing under an earlier contract (ref. 3-5) and was first used by DOT/TSC for their balloon test program during 1971.

3.2.2 Satellite Link Configuration

All U.S. aeronautical technology tests were conducted between the FAA KC-135 airplane and the NASA/Rosman ground station via the NASA geostationary ATS-6 satellite using the basic link configuration of figure 3-2. All antenna evaluation tests were performed with a one-way forward-link configuration. The test signal was transmitted from the Rosman ground station to the ATS-6 satellite for relay to the KC-135. For antenna tests, the test signal consisted of an unmodulated cw carrier transmitted at a constant power level throughout the test. Additional forward-link channels were normally transmitted to allow other L-band participants to conduct other tests concurrently. Return-link voice transmissions from the KC-135 were used only for test coordination purposes when needed. To guard against possible

²Design features of the TOP/LWSD/RWSD slot dipoles are described in more detail in "U.S. Aeronautical L-Band Satellite Technology Test Program – Terminal Design," material submitted under contract DOT-TSC-707, August 1975.

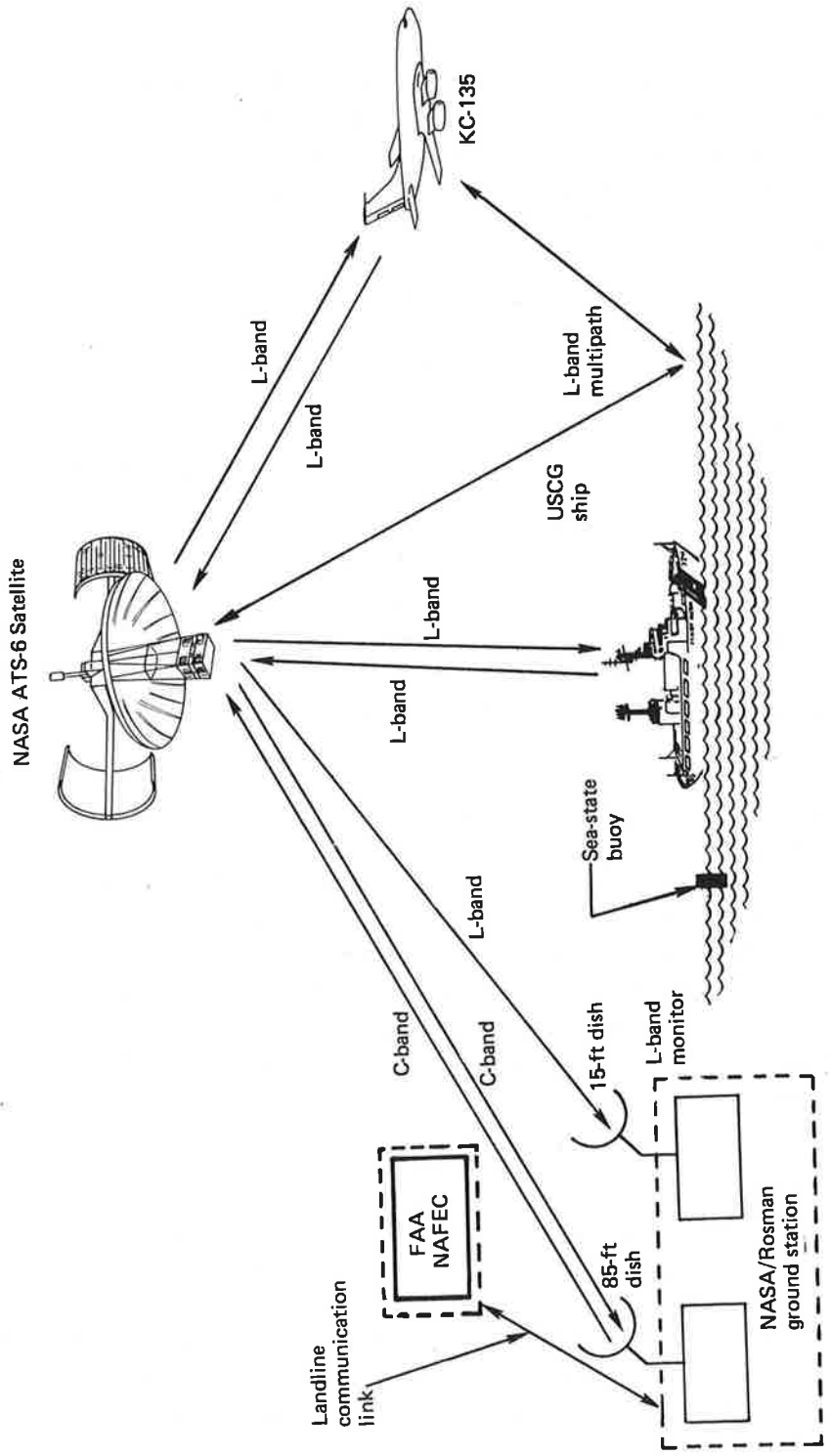


Figure 3-2. Link Configuration for DOT ATS-6 L-Band ATC Experimentation and Evaluation Tests

signal interference, these transmissions were made using antennas (i.e., RSD/LSD) other than those under test.

The ATS-6 satellite transponder was operated in the coherent phase-locked mode for all antenna evaluation tests. The forward reference carrier needed for coherent mode operation was normally transmitted from the NASA/Mojave ground station. This mode of operation referenced the L-band forward-link frequencies to a highly stable ground-based standard, thus eliminating any frequency uncertainty and drift associated with the satellite internal master oscillator.

3.2.3 KC-135 Terminal Configuration

The KC-135 terminal instrumentation was designed and implemented with sufficient capability and flexibility to perform all the various ATS-6 aeronautical L-band satellite technology and demonstration tests without extensive reconfiguration. Capability for rapid changes from one test configuration to another was required since several test types were usually conducted on any given flight.

For antenna evaluation tests, the KC-135 terminal provided two independent receiving channels for simultaneous reception of the same downlink signal via two separate antennas. Compared with a single-channel receiving system, this dual-channel configuration had several advantages: (1) it obtained more data in a given time period, (2) it allowed the antenna under test to be compared with the quad-helix "gain reference" for real-time gain calibration, and (3) it yielded the true relative performance of the two antennas under test.

A simplified block diagram of the KC-135 terminal is shown in figure 3-3. Either the quad helix or the selected slot dipole could be connected to the PLACE receiver and either the phased array or patch could be connected to the other receiving system. After amplification and down-conversion to 10 MHz, the two signals were time multiplexed, at a 3-sec switching rate, to an envelope detector. The detected output was recorded for off-line computer analysis to determine C/N_0 and S/I for each receiving system. Two spectrum analyzers and several other instruments were used for system monitoring, calibration, and real-time performance measurements. An eight-channel chart recorder provided a hard-copy log of selected in-flight reference data. The terminal configuration is discussed in more detail in the following sections.

3.2.3.1 RF Channel Description – Each RF receiving channel for antenna evaluation tests includes a directional coupler, a bandpass filter, and a transistor preamplifier, followed by an L-band receiver. The directional coupler allows calibrating signals consisting of noise and/or a simulated ATS-6 signal to be injected into the receiving channel for system operating noise figure measurement, system performance calibration, and terminal pretest checkout. The low-noise transistor preamplifier ensures that an adequate C/N_0 can be achieved for low-gain antenna testing. The L-band receivers perform the frequency down-conversion and IF amplification required. All amplification is linear without automatic gain control

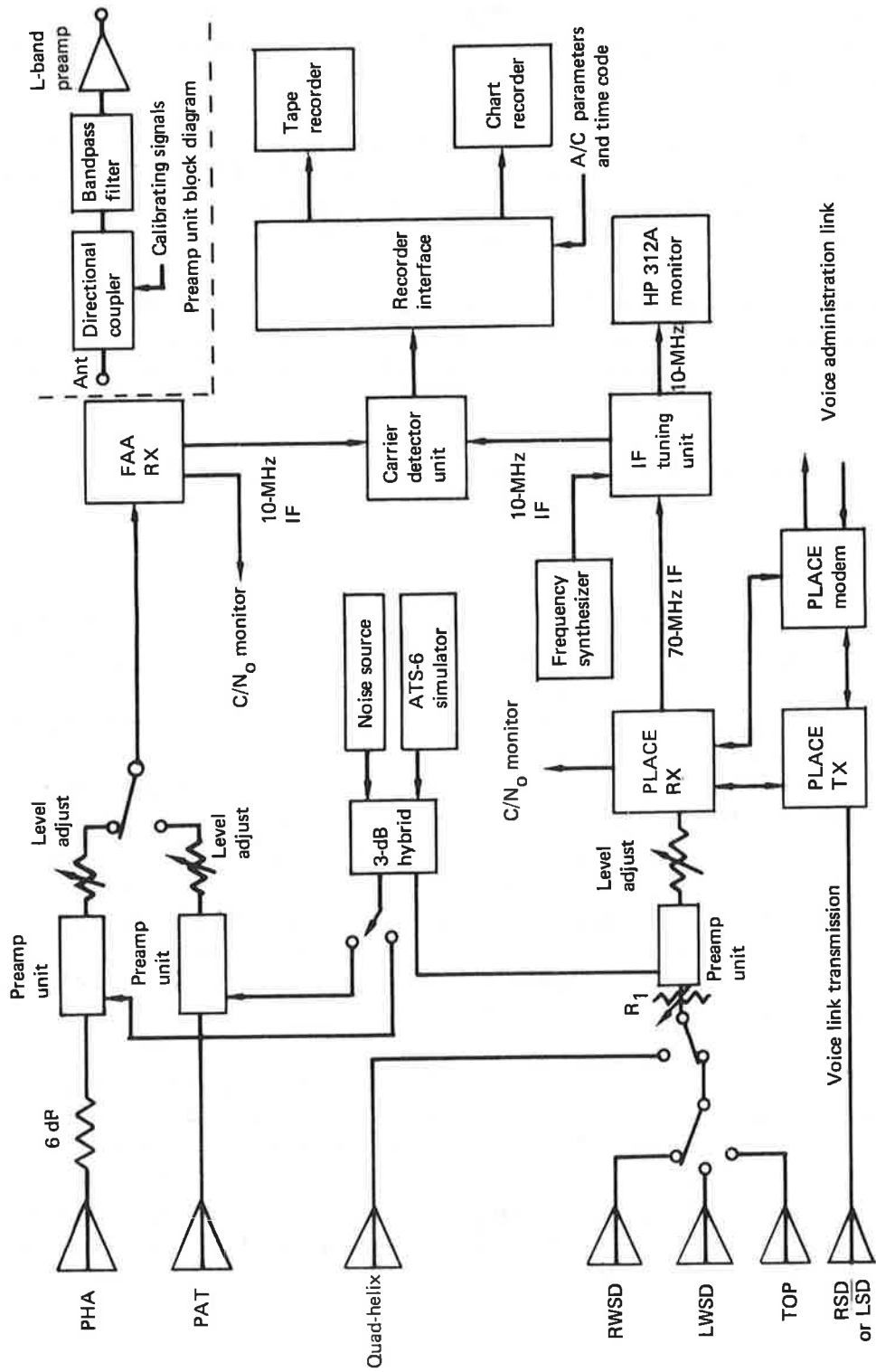


Figure 3-3. Simplified KC-135 Terminal for Antenna Evaluation Test

(AGC) throughout the two receiving systems. The PLACE receiver down-translates to 70 MHz, while the FAA L-band receiver down-translates to 10 MHz. The FAA L-band receiver also provides IF tuning and signal level control for that receiving channel.

Because of both hardware and software considerations, greatest accuracy is achieved during data analysis if the received C/N_0 is within the range of approximately 42 to 52 dB-Hz and if the dynamic range of level variations or level differences between the two receiving channels is less than about 10 dB. Calibrated RF step attenuators are therefore incorporated into the RF subsystem design. The two attenuators preceding the preamplifiers in figure 3-3 allow reduction of the received C/N_0 to the desired range when high-gain antennas are used, whereas the attenuators following the preamplifiers permit signal level equalization for different antenna systems. Because of the high gain of the RF preamplifiers, the attenuators following the preamplifiers allow the levels to be controlled while having negligible effect on the C/N_0 value.

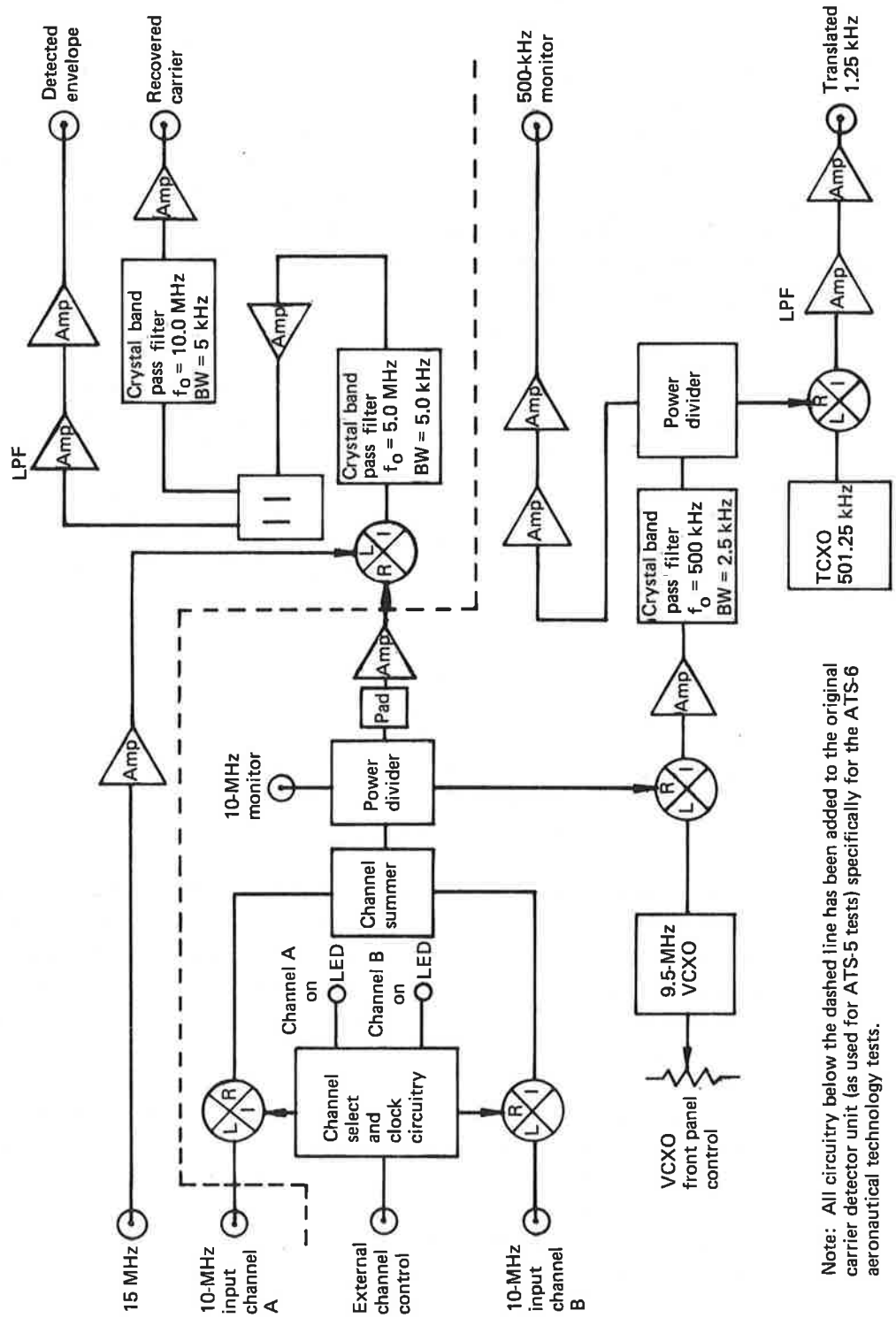
The RF switching and attenuation functions are performed within the aft RF control unit. Detailed design information for this unit and for the preamplifiers is described in unpublished contractual material.³

3.2.3.2 IF Subsystem and Carrier Detector Unit – The down-translated 70-MHz IF from the PLACE receiver is applied to the IF tuning unit for further amplification and down-translation to 10 MHz

The IF tuning unit contains four individually tuned channels for demultiplexing the frequency-division-multiplex (FDM) forward-link spectrum to provide correctly tuned test signals at the desired level for the carrier detector unit and for each modem under test when modem evaluation is performed. Each tuning channel uses a combination of internal fixed local oscillators and a tunable reference frequency derived from an external synthesizer. Outputs at 70 and 10 MHz as required for the various modems and monitoring functions are thus provided. Isolated outputs for test and monitor purposes are available at selected intermediate and output points. For the antenna evaluation tests, only tuning channel 3 was used. This channel provides two identical isolated 10-MHz IF outputs. One is connected to the carrier detector unit input, the other is applied to the HP 312A tuned voltmeter for monitoring signal strength, C/N_0 , and frequency.

The two 10-MHz IF signals, from the IF tuning unit and from the FAA L-band receiver, are connected to the carrier detector unit where they are alternately detected at a 3-sec switching rate. The carrier detector unit was originally designed and fabricated for the FAA ATS-5 test under contract DOT FA69WA-2109. For the ATS-6 aeronautical technology tests, the unit was modified to provide for time multiplexing the two 10-MHz input channels and to provide an additional baseband signal monitoring channel. A functional block diagram of the unit is shown in figure 3-4. The two 10-MHz input

³See footnote, page 3-4.



Note: All circuitry below the dashed line has been added to the original carrier detector unit (as used for ATS-5 tests) specifically for the ATS-6 aeronautical technology tests.

Figure 3-4. Carrier Detector Unit

channels, A and B, can be individually selected manually by the channel select network, which also incorporates timing circuitry to allow alternate selection of the two input channels at one of several switching rates. Signal mixing does not occur since the switches performing the multiplexing provide high isolation between channels. A three-way power divider distributes the received 10-MHz IF signal to the envelope detector channel, the frequency down-translation channel, and a 10-MHz monitor point. The envelope detector output is recorded for off-line computer analysis. Best performance of the envelope detector is achieved if the IF signal input level to the carrier detector unit is within the range of -12 to -28 dBm. The IF input levels of the two channels were therefore carefully adjusted to the desired nominal values during the pretest setup procedures.

3.2.3.3 Data Recording Subsystem – The envelope detector output (carrier detector C/N_0), carrier detector unit channel selection switching (multiplexing) gate, IRIG-B time code, aircraft flight parameters, and voice messages on the administrative air/ground voice communication link were recorded on one of two 14-track instrumentation recorders. The aircraft flight parameters – heading (coarse and fine), roll angle, pitch angle, and altitude – were multiplexed onto one track using standard IRIG sub-carrier FM recording techniques. Single-carrier wideband FM-record channels were used for the envelope detector output and carrier detector switching gate. All channels being recorded were also played back concurrently to allow the recording process to be monitored.

An eight-channel HP 7814A chart recorder provided a hard-copy log of selected reference data signals. The signals recorded included envelope detector output, carrier detector multiplexing gate, HP 312A wave analyzer output, and HP 3590 wave analyzer output. The manually logged data includes time marks for events such as antenna changeovers, aircraft heading, antennas under test, and any test anomalies or departures from the test operations plan.

3.2.3.4 Calibration and Monitoring Instrumentation – A channel calibration and monitoring scheme was implemented to perform terminal functional checkout, calibration, troubleshooting, and real-time measurements. The system design incorporated a channel calibrator capable of injecting either a simulated ATS-6 signal or wideband noise from a calibrated noise source into the input of each receiving channel. The simulated ATS-6 signal was used for terminal checkout, calibration, and troubleshooting. The noise source is used for noise figure measurement and rapid checks of receiving channel continuity.

Equipment used for real-time measurements included (1) two HP 141T spectrum analyzers for measuring and monitoring the C/N_0 , signal level, and frequency at the receiving system 70-MHz IF points, (2) an HP 312A selective voltmeter and HP 3590A wave analyzer for similar measurements at the 10-MHz and 500-kHz IF monitor points of the IF tuning and carrier detector units, and (3) several oscilloscopes. The spectrum analyzers (or HP 312A) were also used as indicators, in conjunction with the channel calibrator, during receiving system noise figure measurements.

3.3 FLIGHT TEST AND PLANNING PROCEDURES

3.3.1 Test Geometries and Scenarios

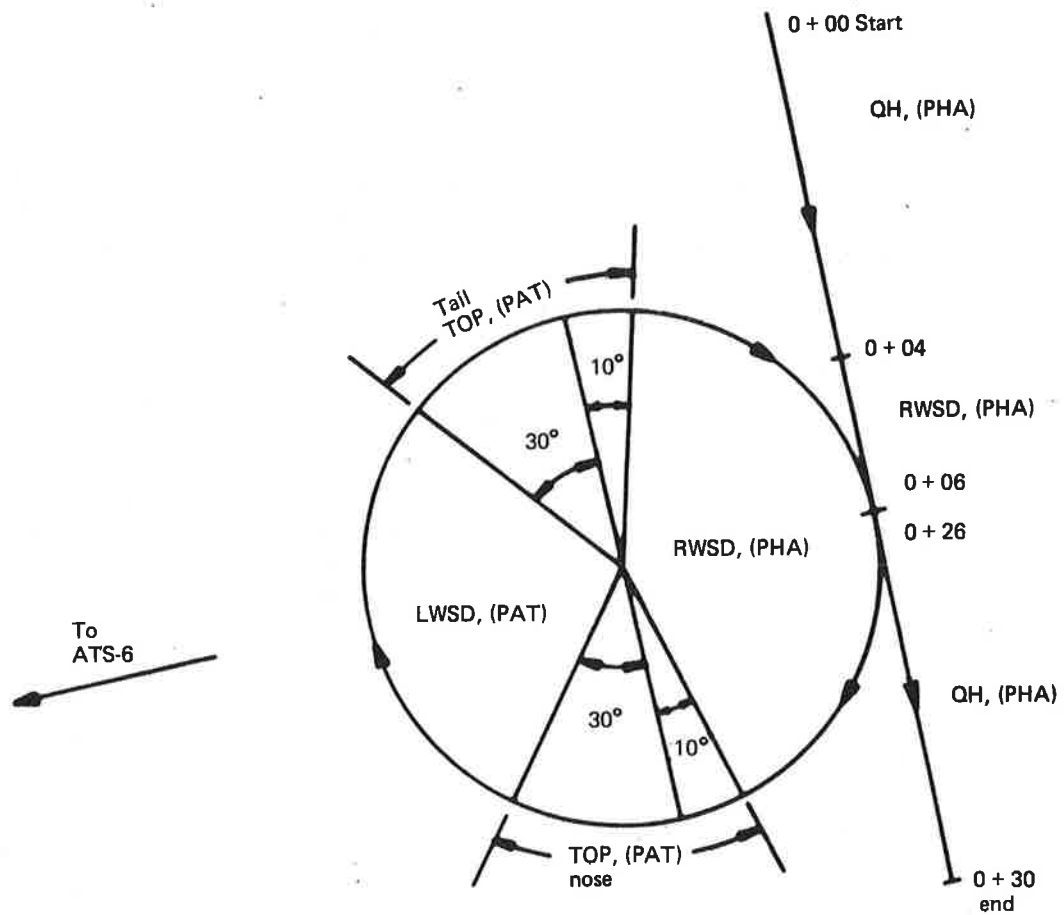
Two types of flightpaths, circular and linear segments, were used to acquire antenna performance data at elevation angles ranging between 10° and 40° . Except for a few tests conducted with the aircraft parked on the ground, all tests were overocean in order to assess performance in the overocean multipath environment.

For circular flightpaths, the airplane was flown in a large circle (20-nmi radius) with near-zero bank angle, thus acquiring antenna data on a quasi-continuous basis. Figure 3-5 gives the basic test geometry and scenario.

A circular-path test began with a 6-min linear flight segment broadside to the satellite direction. During the first 4 min of this segment, the quad helix was connected to one receiving system while the phased array was connected to the other. After the QH pointing was optimized and PHA elevation beam position was selected, final signal level adjustments were made and data was acquired, with the carrier detector unit multiplexing between the PHA and QH channels. During the final 2 min of the initial calibration portion, the QH was replaced by the RWSD. At $t_0 + 06$, the aircraft began its turn at a planned turn rate of 18° per minute (completion of circle in 20 min). During the turn the aircraft heading was continuously monitored and antenna changeovers (as indicated in fig. 3-5) were made when the aircraft heading relative to the satellite reached the value specified in the test operations plan for the flight. Throughout the circular portion of the test, one receiving system acquired data for the three-element slot-dipole antennas while the other acquired data for the phased-array/patch combination. No further PHA elevation beam position optimization was performed subsequent to the initial calibration period. After the circle was completed, a 4-min straight-line segment was flown to allow verification and "backup" for the initial calibration period at the start of the test.

The instrumentation recorder was operated continuously throughout the test. Major events and timing were identified on the chart recorder, which served as a log during detailed off-line analysis of the data recorded on magnetic tape.

During the 1974 fall series, seven such tests were planned at elevation angles ranging between 10° and 40° . However, it was found that (1) the circular path was difficult for the flight crew to fly successfully and (2) the continually changing heading made manual C/N_0 measurements (deemed useful as a check on the subsequent analysis) difficult to make accurately. During the data analysis it was also discovered that the "conical" cuts through the phased-array beam did not acquire all the data desired because of the characteristic beam shape of the antenna. The characteristic beam shape was such that a number of elevation beam positions had to be selected in order to achieve maximum gain as the relative bearing angle to the satellite was changed. Typically, two or three different elevation beam positions, depending on the satellite elevation angle, were required to maintain optimum reception during a 90°



Test segment	Hdg. relative to ATS-6	PLACE RX	FAA RX
Initial calibration	270°	QH, RWSD	PHA
Circle	270° to 350°	RWSD	PHA
	350° to 30°	TOP	PAT
	30° to 150°	LWSD	PAT
	150° to 190°	TOP	PAT
	190° to 270°	RWSD	PHA
Circle	270°	QH, RWSD	PHA
Final calibration			

Figure 3-5.—Antenna Evaluation Test Geometry

heading change from the broadside direction. Continual optimization of phased-array elevation beam steering during circular flight was considered to be undesirable from a test conduct viewpoint and would also be undesirable during the subsequent data analysis. The narrow roll-plane 3-dB beam width (typically between 12° and 15°) of the PHA caused the received signal strength to be rather sensitive to aircraft roll motions,⁴ thus adding to the difficulty of acquiring phased-array data during circular flight.

As a result, additional antenna tests based on linear, rather than circular, flightpaths were designed specifically to acquire data for the phased array. For these tests, conducted during the spring 1975 series, the planned flightpath consisted of seven straight-line segments, each of 13-min duration. The segments were offset 0° , 30° , 60° , 90° , 120° , 150° , and 180° relative to ATS-6 on the right side of the aircraft. These segments were easy to fly and were of sufficient time to allow phased-array antenna beam selection optimization as well as manual measurement of C/N_o and gain calibration. Data were also acquired for the three-element slot-dipole and patch antenna systems during these tests.

The linear flightpaths had several disadvantages compared with circular paths: (1) less efficient use was made of satellite and flight time, (2) data was available at 30° azimuthal increments only, rather than quasi-continuously, (3) the total flightpath spanned a much larger geographic region over which the ATS-6 antenna gain coverage may not be entirely constant, and (4) the duration of the test was much longer, increasing the possibility of ATS-6 RF power output variation during test conduct. Because of these limitations, the circular flightpath was used for all antenna evaluation tests for which the primary objective was the acquisition of data for operational-type antennas such as the slot dipoles. Several additional circular-path tests were conducted during the spring test series.

3.3.2 Real-Time Calibration Measurements

Real-time measurements are needed to ensure that the receiving systems are functioning normally and to provide redundant data that can be compared with the results of off-line data analysis for validation purposes. The most important measurements are system operating noise figure (NF_{op}), signal-to-noise power density ratio (C/N_o), signal level, frequency, and aircraft heading.

3.3.2.1 System Operating Noise Figure Measurement – The system operating noise figure measurements were made by a standard manual Y-factor technique. A complete measurement involves excess noise ratio (ENR) calibration, Y-factor measurement, and NF_{op} computation.

⁴Circular flightpaths were normally flown with the autopilot disengaged; hence aircraft roll motions are typically slightly larger than during linear flights, the latter normally being flown with the autopilot engaged. Even during circular flights, however, recorded data shows that average roll angles were usually less than 3° , with peaks only occasionally exceeding 5° . Roll sensitivity was therefore not a serious problem and was not a strong consideration in the scheduling of additional linear-path tests.

Noise is injected into the receiving system from a calibrated L-band noise source by means of the directional coupler preceding the preamplifier. The noise source output ENR was calibrated in the laboratory using a hot-cold source. Two separate methods were used to calibrate the effective excess noise level injected into the receiving system referred to the preamplifier input reference point used for defining NF_{op} . The first method is based on calibration of the total RF path insertion loss (IL) between the noise source and the transistor preamplifier. The RF path includes the 3-dB hybrid, connecting cables, bandpass filter, and directional coupler as shown in figure 3-3.

The effective ENR at the reference point can then be computed as follows:

$$ENR_{eff} = ENR_o - IL \quad (3-1)$$

where:

ENR_o = calibrated ENR (29.6 dB) of the noise source
 IL = total insertion loss

The second method used to calibrate the effective ENR at the reference point is based on terminating the input port (the port connected to the antenna) of the directional coupler so that the system operating noise figure is then equal to the intrinsic noise figure of the transistor amplifier. The effective ENR can then be calculated from

$$\begin{aligned} ENR_{eff} &= NF_{op} + 10 \log_{10} (Y-1) \\ &= NF_{TR} + 10 \log_{10} (Y-1) \end{aligned} \quad (3-2)$$

where:

NF_{TR} = known intrinsic preamplifier noise figure (also calibrated in the laboratory)
 Y = measured Y-factor when the noise source is turned on and off

Since the first technique discussed above is time consuming, it was usually applied only during ground system calibration to verify the result obtained by the second technique. The second technique was used as the standard method for preflight calibration.

3.3.2.2 C/N_o Measurement, Frequency Monitoring, and Level Monitoring – The instruments used for C/N_o measurements were the HP 141T spectrum analyzer and HP 312A wave analyzer. They were normally connected at 70-MHz IF and 10-MHz IF, respectively. The C/N_o measurement technique involves true rms measurement of noise power with an instrument of calibrated noise bandwidth.

Applicable correction factors are applied for the spectrum analyzer and wave analyzer detector characteristics and filter noise bandwidths.

The input IF bandwidth of the carrier detector unit is 5 kHz and the input frequencies must be held well within this bandwidth. Independent frequency monitors are therefore applied to the two 10-MHz IF inputs to the carrier detector unit. A single instrument, i.e. HP 312A wave analyzer, is used to monitor both the amplitude and center frequency of the channel A signal, which is provided by the IF tuning unit. The frequency is tunable by adjusting the external synthesizer to the IF tuning unit, and the amplitude may be varied by the IF gain at the IF tuning unit.

The center frequency and amplitude of the 10-MHz signal from the FAA L-band receiver are monitored by using the internal coherent amplitude detection (CAD) circuitry of the receiver. A precision-tuned 10-MHz VCXO can track the signal by employing phase-lock carrier tracking. Any frequency offset is directly readable from the front panel loop stress indicator. The same channel provides a calibrated dc output that is proportional to the input signal amplitude. This dc signal may be displayed on an oscilloscope to monitor the IF signal level relative to the nominal level desired at the input of the carrier detector unit.

Each of these techniques provided a continuous indication of input frequency and level, with accuracy and resolution well in excess of the requirements. Frequency changes due to downlink frequency drift were negligible due to the coherent mode operation of the satellite. Adjustments were required only because of Doppler due to aircraft velocity changes relative to the satellite direction. Only occasional incremental corrections were required during a circular flightpath.

3.4 ANTENNA TEST DATA ACQUISITION SUMMARY

A summary of the antenna evaluation tests conducted is given in table 3-1. All antenna tests were conducted as planned except on two occasions when significant deviations from the test operations plan occurred. On October 1, 1974, the test was to be conducted within warning area W-107, just offshore from NAFEC. Due to in-flight delays, the aircraft did not arrive at the designated test area on schedule and could not carry out the scheduled test because of ATC conflicts at the actual aircraft location. On January 21, 1975, the aircraft could not attempt takeoff because of an icy runway; consequently, a ground test was conducted at various bearing angles by taxiing the aircraft at NAFEC.

TABLE 3-1. ANTENNA EVALUATION DATA ACQUISITION SUMMARY

Date, mo/day/yr	Elev angle, deg	Flight geometry	Test duration, hr + min	Antenna tested	Remarks
9-24-74	30	Circular	0+30	SDP, PHA	As per figure 3-5
10-01-74	40	Circular	0+30	SDP, PHA	Flightpath deviations due to ATC conflicts
10-23-74	25	Circular	0+30	SDP, PHA, PAT	As per figure 3-5
10-24-74	19	Circular	0+30	SDP, PHA, PAT	As per figure 3-5
10-29-74	15	Circular	0+30	SDP, PHA, PAT	As per figure 3-5
11-21-74	19	Circular	0+30	SDP, PHA, PAT	As per figure 3-5
1-21-75	40	Linear	1+50	SDP, PHA, PAT	Ground test at NAFEC, various headings by taxiing aircraft
1-22-75	9	Linear	0+30	SDP, PHA	Three segments
1-27-75	17	Linear	1+30	SDP, PHA, PAT	Seven segments
3-25-75	15	Circular	0+20	SDP	Bad weather
3-27-75	14	Linear	1+30	SDP, PHA, PAT	Seven segments
4-01-75	15	Circular	0+20	SDP	Bad weather

4. DATA ANALYSIS DESCRIPTION

The parameters required for presentation of antenna evaluation test results are antenna gain, signal-to-multipath interference ratio (S/I), elevation angle, and relative bearing angle to ATS-6.

The S/I ratio and C/N_0 value for each receiving channel, along with aircraft heading and pitch and roll angles, were determined from data recorded on the magnetic tape. Calculation of antenna gain used the computed C/N_0 values, augmented by NF_{op} measurements and RF subsystem line loss calibration measurements.

4.1 DATA ANALYSIS PROCEDURES

As a first step in data processing, analog tapes were digitized at the Boeing Test Data Processing Center (TDPC) to provide computer-compatible seven-track 800-bpi digital tapes. Aircraft heading, pitch, and roll plus time code were stripped out on chart paper, as shown in the example of figure 4-1. The digital tapes were then processed further by the CDC 6600 to determine C/N_0 and S/I.

4.1.1 Bearing and Elevation Angles Computation

The satellite elevation angle is computed from fundamental trigonometry using the known satellite and aircraft locations. The relative bearing angle to the satellite was computed from the stripouts of aircraft magnetic heading (fig. 4-1) used in conjunction with the known satellite direction and magnetic variation at the test location.

Aircraft roll angle stripouts were examined whenever such information was available, and data points were discarded if roll exceeded $\pm 5^\circ$. During normally executed flights, the aircraft roll angle exceeded $\pm 5^\circ$ only on infrequent occasions (see fig. 4-1); hence data purges due to aircraft roll constituted only a small percentage of the data base. Aircraft pitch angle was normally between 4° and 6° (nose up) during data acquisition. This flight attitude is normal at the altitude and velocity conditions (30,000 ft, 375 kn) employed for antenna tests. No adjustments (or data censoring) were made due to pitch angle considerations.

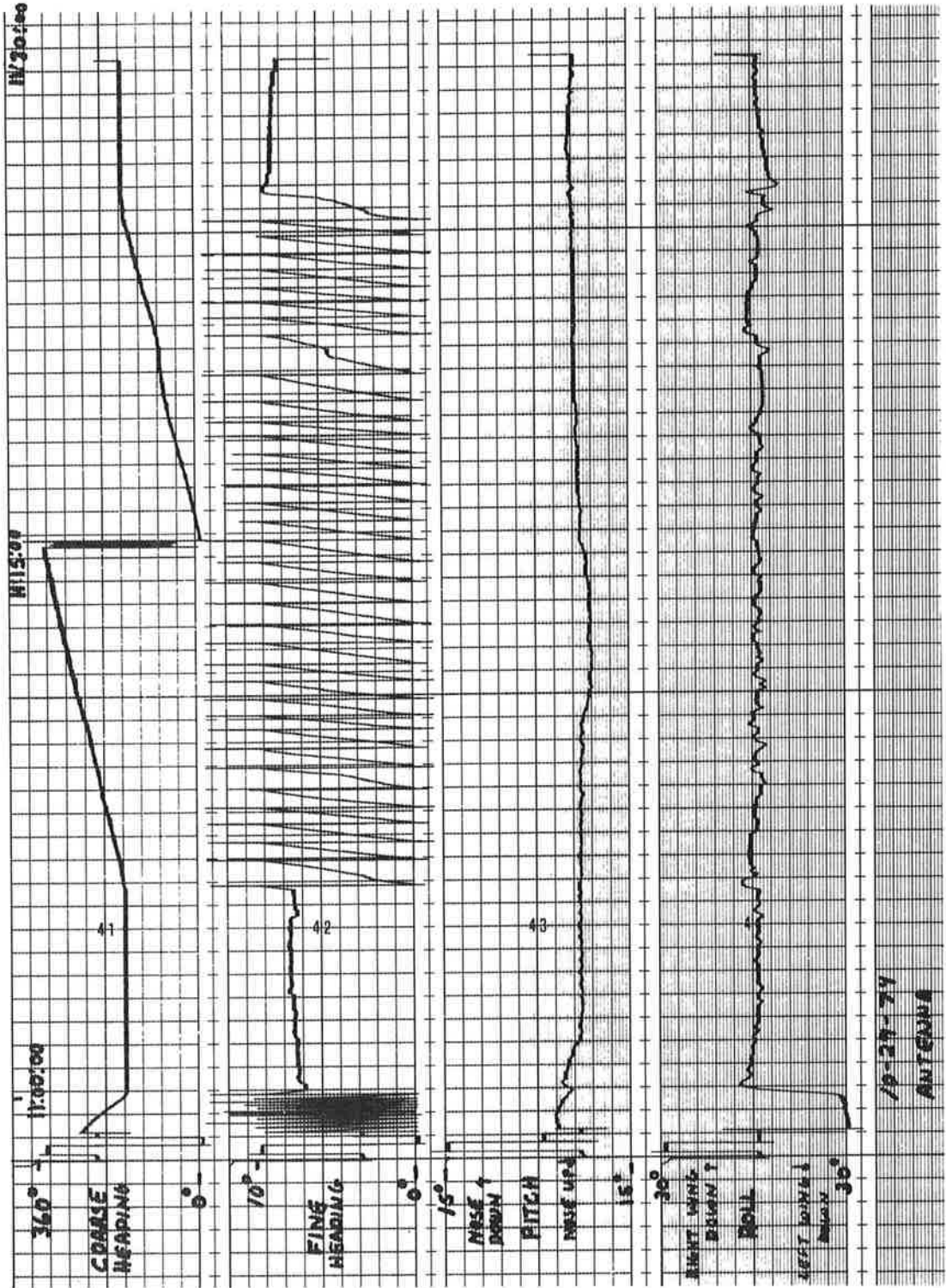


Figure 4-1. Aircraft Heading Pitch and Roll Data, October 29, 1974

4.1.2 C/N₀ and S/I Determination

The calculation of C/N₀ and S/I is basic to all antenna evaluation and modem tests. The cw carrier transmitted from Rosman to the aircraft via ATS-6 was processed by the envelope detector in the carrier detector unit. The detected envelope output was FM recorded and computer analyzed to determine C/N₀ and S/I. A detailed description of the mathematical basis for this analysis and the algorithms used are given in volume IV of this report. The data acquisition procedures and algorithm make it possible to obtain these estimates as often as every 3 sec for antenna tests.

Specifically, the envelope-detected signal was digitized at a 2-kHz rate using 10-bit quantization to obtain 1025 signal strength samples in approximately 0.5 sec. The 1025 samples were processed to remove sample bias and linear drift components. The sample mean (\bar{S}), mean square values (S^2), and variance (σ^2) were then determined. After the time-domain samples were tapered to minimize spectral window side-lobe peaks, the discrete Fourier transform was performed on the time-domain data using a fast Fourier transform (FFT) algorithm. The output of the FFT provided power spectral density versus frequency for the range 0 to 800 Hz.

The output spectrum can be expanded as a mathematical series involving direct signal power, multipath spectrum, and the noise spectrum. The spectral data was used to calculate a quantity termed "noise floor," which was computed as the weighted average of the spectral density from 250 to 800 Hz. This frequency range was chosen with the a priori knowledge that there will be little multipath power above 250 Hz in comparison to noise power. The ratio of the squared mean signal strength to the noise floor value was calculated to determine C/N₀ using a computer look-up table. The look-up table was based on analytical modeling of the carrier detector output. The modeling has been experimentally verified for the additive noise environment. The experimental verification data and a detailed analysis are given in volume IV of this report.

S/I ratios of up to 20 dB (which represents the multipath resolution capability of the analysis technique) can be estimated. To estimate S/I, the spectral data was numerically integrated from 2 to 250 Hz to yield a band-limited variance figure caused by the combined effects of multipath power and noise. This calculation uses the a priori knowledge that virtually all multipath-related energy will fall within the range of 0 to 250 Hz. The ratio of squared mean to the above band-limited variance was calculated and used together with C/N₀ to estimate S/I by graphical methods. These graphical relationships were also based on analytical modeling.

4.1.3 Antenna Gain Calculation

The relative gain of the antennas can be deduced by comparing the received power levels at the antenna terminals. Furthermore, absolute gain can be estimated by using the quad helix as a

standard, since it is known to provide 15.5-dB gain to RHC-polarized signals when optimally pointed. As a first step in calculating antenna gain, the value of the receiving system equivalent noise power density, N_o , referred to the antenna terminals was determined. The applicable equation is

$$N_o = -204.0 + L_t + NF_{opm} \quad (4-1)$$

(dBW/Hz) (dBW/Hz) (dB) (dB)

where:

- L_t = total RF losses between the antenna terminals and the preamplifier input terminal, as determined from RF subsystem calibration measurements
- NF_{opm} = measured receiving system operating noise figure referred to the preamplifier input terminals

The received signal strength, S_A , at the antenna terminals is then calculated from the measured C/N_o and the N_o value determined above; i.e.,

$$S_A = C/N_o + N_o \quad (4-2)$$

(dBW) (dB-Hz) (dBW/Hz) .

The unknown gain, G_A , of an antenna under test can then be determined from

$$G_A = G_{QH} - (S_{QH} - S_A), \text{ dB} \quad (4-3)$$

where:

- G_{QH} = known gain of reference QH antenna (dB)
- S_{QH} = received signal strength at QH output terminals (dBW)
- S_A = received signal strength at output terminals of antenna under test (dBW)

Quad-helix gain calibration data, i.e., S_{QH} , was not available for all segments since (1) quad-helix azimuthal steering was restricted to $\pm 110^\circ$ from the nose and (2) operational procedures and RF subsystem hardware constraints sometimes precluded acquisition of quad-helix reference gain data. However, additional information was available from signal strength measurements made during other tests in adjacent time periods. Thus the expected ATS-6 signal strength could be determined for a certain test area, especially along the modem evaluation Type II test path at an elevation angle of 15° . Such data have been used on occasion to augment the normal quad-helix antenna gain calibration data,

especially during those portions of the linear-path flights for which the quad helix could not be pointed toward the satellite. Specific occasions are identified in later sections where test results are presented.

Channel characterization data for all antenna evaluation receiving channels is tabulated in table 4-1. The total RF insertion loss, L_t , between an antenna and a transistor preamplifier includes losses in the transmission line, RF step attenuator, directional coupler, and a bandpass filter. Calibration measurements were made on the installed system in the aircraft to determine the values of L_t . NF_{opm} denotes the measured system operating noise figure referred to the input port of the transistor preamplifier. The summation of these two quantities yields the quantity "effective NF_{opa} " from which the value of N_o (eq. (4-1)) follows directly.

TABLE 4-1. RECEIVING CHANNEL CHARACTERIZATION FOR ANTENNA EVALUATION TEST

RF Path		L_t dB	NF_{TR} dB	Measured NF_{opm} dB	T_{a1} K	T_s K	Effective NF_{opa} dB	Est T_{a2} K	NF_{ope} dB
From	To								
LWSD ^a	TR2	3.8	3.0	2.2	56	1,155	6.0	100	2.4
LWSD ^b	TR2	7.4	3.0	2.8	147	3,037	10.2	100	2.7
RWSD ^a	TR2	4.1	3.0	2.2	40	1,237	6.3	100	2.4
RWSD ^b	TR2	7.7	3.0	2.8	137	3,254	10.5	100	2.8
TOP ^a	TR2	4.1	3.0	2.1	12	1,209	6.2	50	2.2
TOP ^b	TR2	7.7	3.0	2.7	63	3,180	10.4	50	2.7
QH ^a	TR2	2.9	3.0	2.2	100	938	5.1	75	2.1
QH ^b	TR2	13.4	3.0	2.95	145	13,514	16.4	75	2.9
PHA ^a	TR4	2.0	3.3	2.1	53	745	4.1	50	2.1
PHA ^b	TR4	8.3	3.3	3.0	46	3,948	11.3	50	3.0
PAT ^a	TR5	2.4	3.3	2.2	49	836	4.6	50	2.2

^aChannel characterization for fall 1974 tests.

^bChannel characterization for spring 1975 tests.

Legend:

- L_t total insertion loss between an antenna and its preamplifier
- NF_{TR} intrinsic noise figure of a preamplifier with a 50-ohm termination at the input point
- NF_{opm} measured system operating noise figure at preamplifier input, antenna connected
- T_{a1} computed antenna noise temperature using L_t , NF_{TR} , and NF_{opm}
- T_s temperature equivalent of effective NF_{opa}
- NF_{opa} system operating noise temperature at antennas $L_t + NF_{opm}$
- T_{a2} a priori estimate of antenna noise temperature
- NF_{ope} estimated system operating noise figure at preamplifier input using L_t , NF_{TR} , and T_{a2} .

4.1.3.1 *Cross-Checks of Measurement Validity* – Although only the foregoing quantities are of direct interest in the computation of antenna gain, several additional columns of data are given in table 4-1. These combinations of measured and calculated quantities serve as cross-checks on the consistency and validity of the basic measurements of NF_{op} , L_t , etc. The quantity NF_{TR} , the intrinsic noise figure of a transistor preamplifier with the input terminated at a 50-ohm load, was measured in the laboratory. The value of NF_{TR} , together with NF_{opm} and L_t , was used to compute the intrinsic antenna noise temperature T_{a1} . The value of T_{a1} computed in this manner was compared with T_{a2} , the a priori estimate of antenna noise temperature. This comparison is a sensitive check on the reasonableness of the measured NF_{opm} and L_t since even small errors in these quantities lead to large errors in the computed antenna temperature.

A second “reasonableness check” was performed by using L_t , NF_{TR} , and T_{a2} to compute an estimated operating noise figure, NF_{ope} , also referred to the preamplifier input. Comparison of this column with the actual measured value of NF_{opm} indicates the close agreement between measured and estimated values, thus demonstrating the consistency of the basic measurements.

4.1.3.2 *Example Gain Calculation* – The following illustrates an example antenna gain computation for data acquired between 1217Z and 1226Z on January 27, 1975, during a linear-path flight segment. The test was conducted at an elevation angle of 17° and a relative bearing angle of 44° .

- a. QH channel $C/N_o = 44.0$ dB-Hz
- b. RWSD channel $C/N_o = 42.0$ dB-Hz
- c. PHA(2) channel $C/N_o = 42.7$ dB-Hz (where the 2 indicates elevation beam position 2 is selected).

By applying applicable data from table 4-1 into equations (4-1) and (4-2), the received signal power at each antenna is

- a. $S_{QH} = -143.6$ dBW
- b. $S_{RWSD} = -151.5$ dBW
- c. $S_{PHA(2)} = -150.0$ dBW.

Based on a known 15.5-dB antenna gain for the QH antenna and applying equation (4-3), the computed RWSD gain is 7.6 dB and the PHA(2) gain is 9.1 dB.

4.1.3.3 *Reference-Gain Antenna* – Inherent in all experimentally derived values of antenna gain is the assumption that the reference quad-helix antenna gain actually achieved during the calibration measurement portion of the flightpath is, in fact, 15.5 dB. The peak gain of the quad-helix antenna has been verified by full-scale measurements on the antenna range on three separate occasions: once prior to initial installation and twice during subsequent removals for antenna servicing and recalibration.

The most recent recalibration was in mid-1974 just prior to installation for the ATS-6 test program. During initial development of the antenna, measurements were made using a 1/20th-scale-model horn antenna installed on a model KC-135 aircraft. These measurements confirmed that the pattern was not significantly affected by the airframe for broadside pointing. It is therefore concluded that the gain characteristics broadside to the aircraft at elevation angles above 15° are closely represented by the full-scale gain measurements referred to above.

4.1.3.4 Reduction of Statistical Fluctuation in Results — For linear flightpaths the aircraft/satellite geometry remains essentially fixed during data acquisition. Therefore, averaging of the computed C/N_0 values was used to reduce the statistical variability associated with individual C/N_0 samples obtained from the detected envelope signal analysis process. Manual real-time C/N_0 measurements were also logged to serve as a check on analyzed results and for use when analyzed results were unavailable.

For circular flightpaths, the aircraft/satellite geometry is continually changing; hence C/N_0 is not constant and averaging of the computed C/N_0 samples cannot be applied directly. Some reduction in the sample variance of C/N_0 fluctuations can be achieved by noting that although C may be changing, N_0 is independent of aircraft/satellite geometry for all practical purposes. An additional computer program is therefore used to compute the average noise floor from the sample values. The C/N_0 values are then computed as the ratio between the signal strength, C , from individual samples and the average noise floor computed over many samples.

4.2 ANTENNA DATA PRESENTATION

An HP 9830A calculator and HP 9862A calculator plotter were used to compute, tabulate, and plot the final results for all circular flight test results. All computations were tabulated as shown in the example of table 4-2. The calculator computed the relative bearing angle, the adjusted C/N_0 (which results when N_0 is averaged as described), the received signal strength, and antenna gain. The GMT of a data sample, computed C/N_0 , and computed S/I were derived from the CDC 6600 processing and were inputs to this computation. The data listed in columns REL BRG, ANT GAIN, and ANT S/I ¹ are plotted in polar form as the standard data presentation format for circular flights. Although the example illustrated in table 4-2 is for the slot dipoles, phase-array and patch antenna data for circular flights were processed and tabulated in a like manner.

¹Since a value of 20 dB represents the resolution limit for the analytical technique used to estimate S/I , all calculated S/I values (resulting from the CDC 6600 analysis) in excess of 20 dB have been plotted at the 20-dB level. In all subsequent plots of S/I , the 20-dB value therefore represents " $S/I \geq 20$ dB."

For linear-segment tests, only a small number of data points are involved. In this case all parameters were manually computed, tabulated, and plotted.

TABLE 4-2. ANTENNA EVALUATION TEST DATA TABULATION EXAMPLE

DATE OF THE TEST : 11/21/74
 LOCATION OF THE TEST : 40 06 NORTH, 40 30 WEST
 THE ELEVATION ANGLE : 19 DEG
 MAG. VARIATION : 21 DEG WEST
 A/C TO ATS-6 BEARING ANGLE : 244.5 DEG TRUE

TIME GMT	MAG HDG (DEG)	REL BRG (DEG)	COMPUT C/N ₀ (DB-HZ)	NOISE CHANGE (DB)	ADJ. C/N ₀ (DB-HZ)	REC'D SIGNAL (-DBW)	ANT GAIN (DB)	ANT S/I (DB)
1502.25	185	81	49.6	0.00	49.6	148.1	7.6	20.0
1502.37	189	77	48.7	0.41	49.1	148.6	7.2	20.0
1502.50	193	73	49.4	0.42	49.8	147.9	7.9	20.0
1503.02	196	70	49.0	0.01	49.0	148.7	7.1	18.0
1503.15	198	68	48.0	0.55	48.5	149.2	6.6	20.0
1503.27	206	60	49.2	-0.36	48.8	148.9	6.9	19.0
1503.40	209	57	48.6	-0.42	48.2	149.5	6.2	17.0
1503.53	217	49	48.4	-0.22	48.2	149.5	6.2	19.0
1504.18	222	44	47.3	-0.51	46.8	150.9	4.8	17.0
1504.30	227	39	46.0	0.21	46.2	151.5	4.3	19.0
1504.42	231	35	46.3	-0.32	46.0	151.7	4.0	20.0
1505.32	240	26	47.2	0.01	47.2	150.5	5.2	20.0
1505.45	243	23	48.9	-0.40	48.5	149.2	6.5	17.0
1505.58	249	17	48.8	0.42	49.2	148.5	7.3	19.0
ABOVE DATA FOR RWSL			AT NF(PREAMP)=2.2 DB AND I.L.=4.1 DB					
1506.10	251	15	45.5	-0.17	45.3	152.4	3.4	14.0
1506.23	259	7	44.6	0.16	44.8	152.9	2.8	13.0
1506.35	262	4	45.6	-0.32	45.3	152.4	3.3	17.0
1506.48	269	357	45.7	-0.28	45.4	152.3	3.5	20.0
1507.00	271	355	45.0	-0.09	44.9	152.8	2.9	18.0
1507.12	275	351	45.0	0.27	45.3	152.4	3.3	20.0
1507.25	279	347	45.5	0.35	45.8	151.9	3.9	20.0
1507.38	283	343	46.1	0.10	46.2	151.5	4.2	20.0
1507.50	288	338	47.2	-0.06	47.1	150.6	5.2	20.0
ABOVE DATA FOR TOP			AT NF(PREAMP)=2.2 DB AND I.L.=4.1 DB					

Legend:

Time GMT:	Time tag of each data record processed by CDC 6600
Mag Hdg (deg):	KC-135 magnetic heading at above time
Rel Brg (deg):	Computed relative bearing to ATS-6 at above time
Computed C/N ₀ :	Computed C/N ₀ (without noise floor averaging) at above time
Noise Change (dB):	Correction to C/N ₀ for noise floor averaging
Adj. C/N ₀ (dB-Hz):	Computed C/N ₀ with noise floor averaging applied
Rec'd Signal (-dBW):	Received signal strength at antenna terminals
Ant Gain (dB):	Computed gain of test antenna at above time
Ant S/I (dB):	S/I value for above time from CDC 6600 analysis.

5. THREE-ELEMENT SLOT-DIPOLE ANTENNA SYSTEM RESULTS

This section presents plotted and tabulated gain and S/I data for the slot-dipole antenna system. Gain and S/I data derived from antenna range measurements are presented for comparison.

5.1 EXPERIMENTAL GAIN AND S/I DATA

Seven circular-path flight tests were conducted for the slot-dipole antenna system. The test conditions are summarized in table 5-1 and results are plotted in figures 5-1 through 5-8.

**TABLE 5-1. SLOT-DIPOLE-ANTENNA CIRCULAR
FLIGHT SUMMARY**

Date	Elevation angle, deg	Figure
Apr. 1, 1975	15	5-1
Mar. 25, 1975	15	5-2
Nov. 21, 1974	19	5-3
Composite ^a	20	5-4
Oct. 24, 1974	19	5-5
Oct. 29, 1974	16	5-6
Sept. 24, 1974	28	5-7
Oct. 23, 1974	25	5-8

^aComposite plot derived from figures 5-1, 5-2, and 5-3.

Results obtained for the April 1 and March 25, 1975, flight tests will be discussed first. These two tests were conducted in the same area at a nominal ATS-6 elevation angle of 15°. Although high-quality received signal strength data for the antennas was obtained on each occasion, aircraft roll and pitch data was not acquired for either of these tests due to a hardware fault associated with operation of the instrumentation gyro sensor. Aircraft heading data was recorded and confirms that both tests were well flown.

Comparison of results reveals gain asymmetry that is opposite for the two tests: on March 25 the measured gain was higher for the right-side antenna while on April 1 the gain was higher for the left-side antenna. This suggests that the aircraft bank angle may have been nonzero and of opposite polarity for the two tests. Closer investigation tends to confirm the plausibility of this argument.

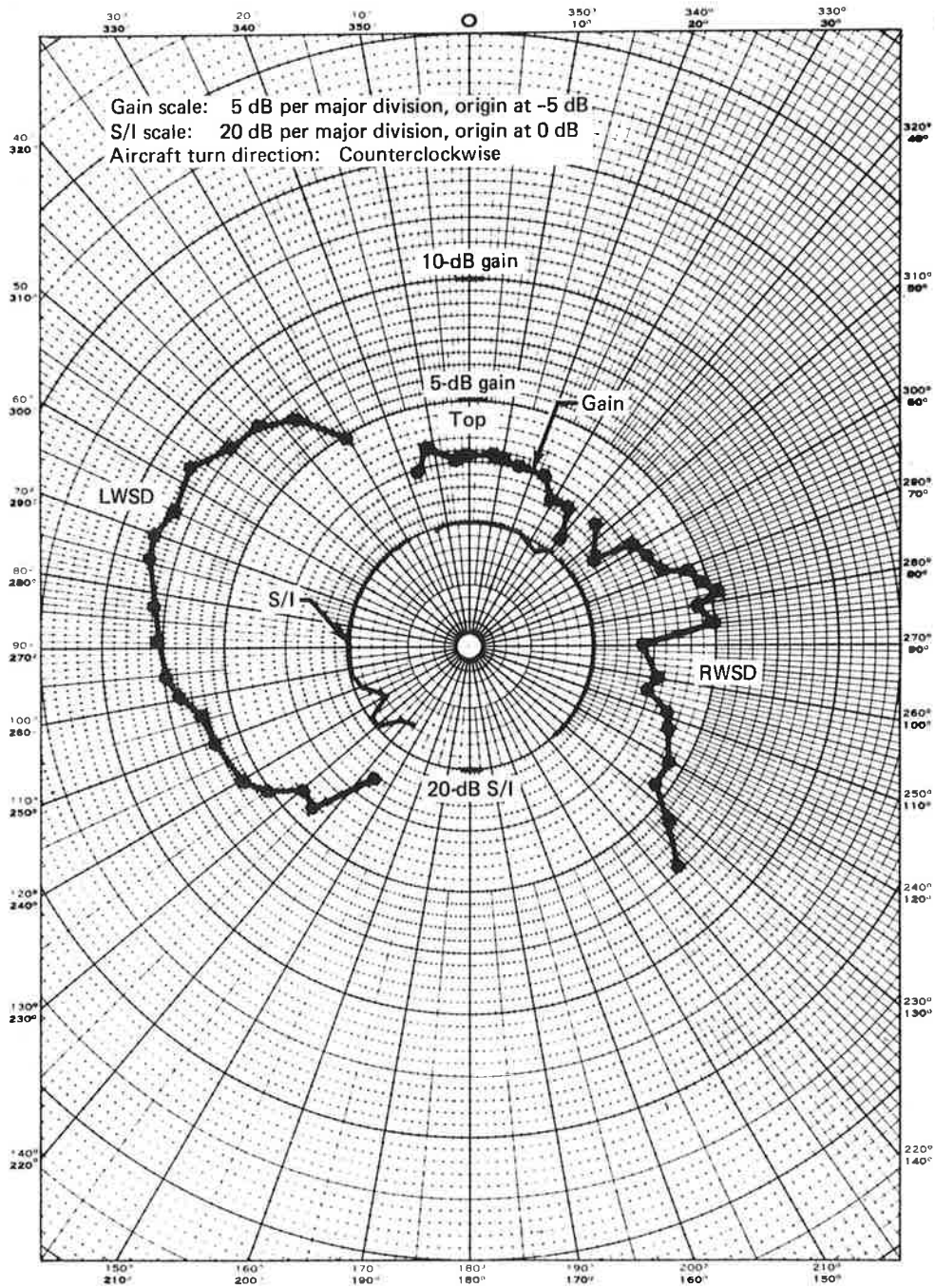


Figure 5-1. Three-Element Slot-Dipole Antenna System Gain and S/I, April 1, 1975, Elevation Angle = 15°

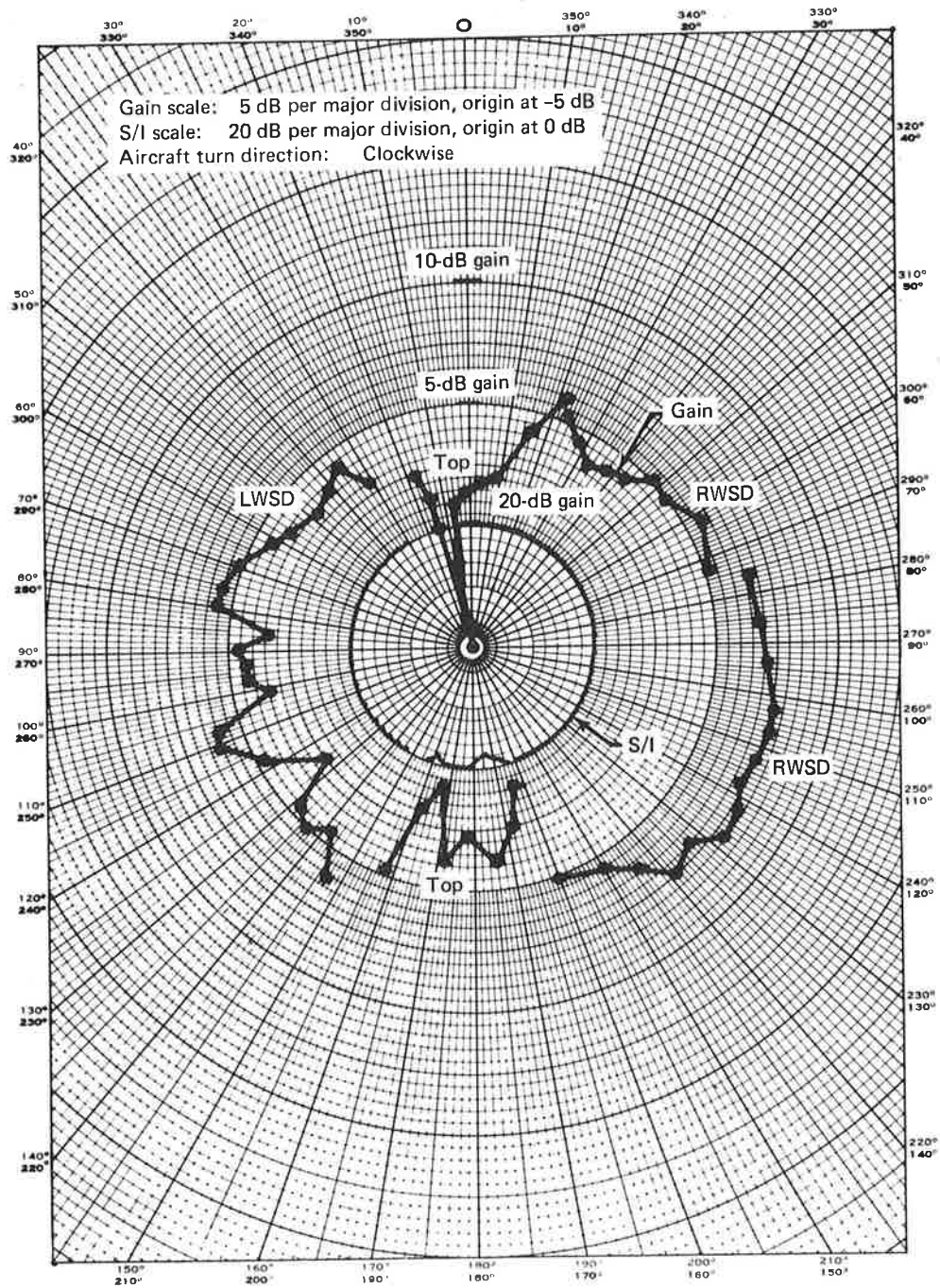


Figure 5-2. Three-Element Slot-Dipole Antenna System Gain and S/I, March 25, 1975, Elevation Angle = 15°

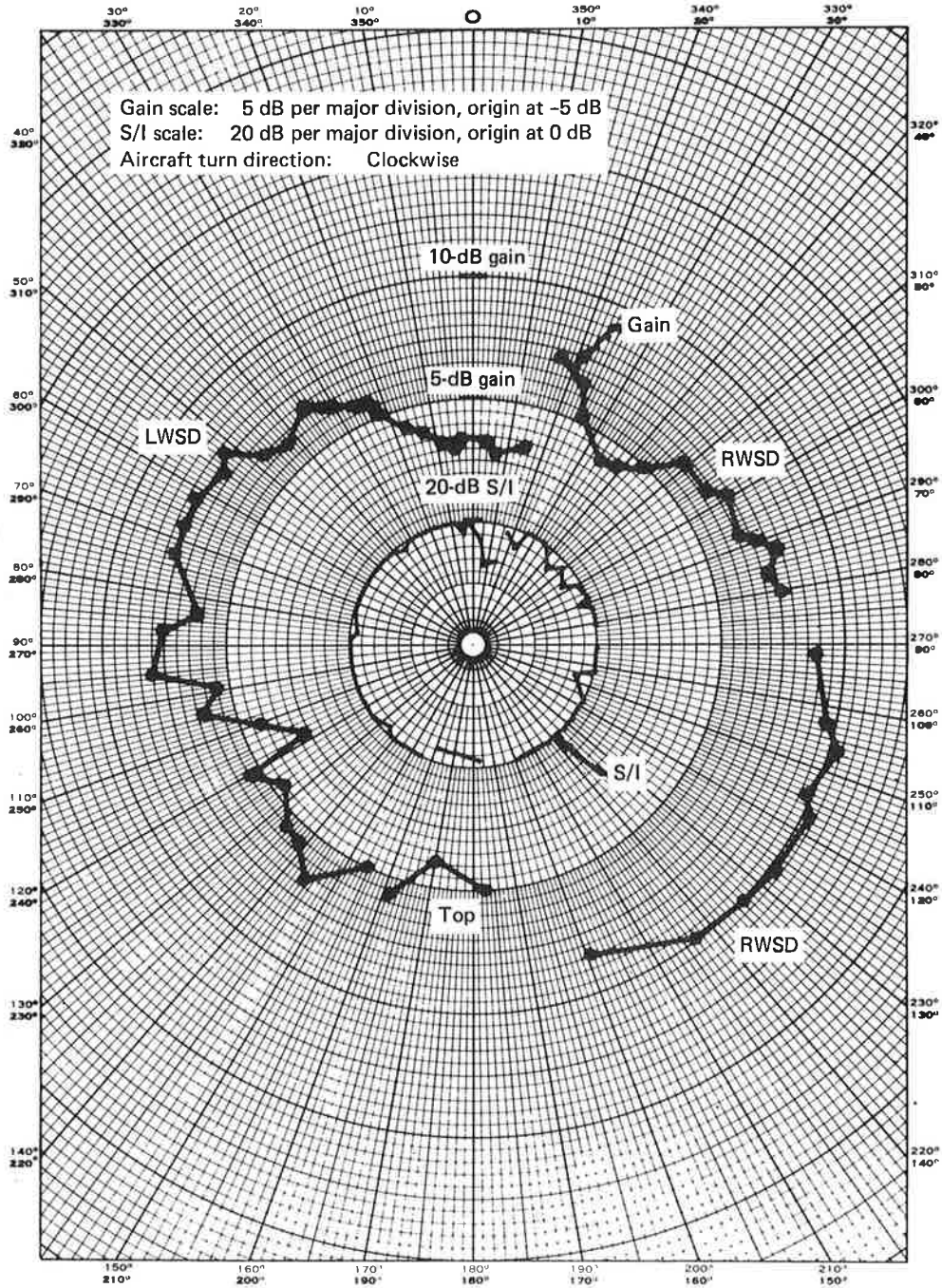


Figure 5-3. Three-Element Slot-Dipole Antenna System Gain and S/I, November 21, 1974, Elevation Angle = 19°

Gain scale: 2-dB per major division, origin at -10-dB

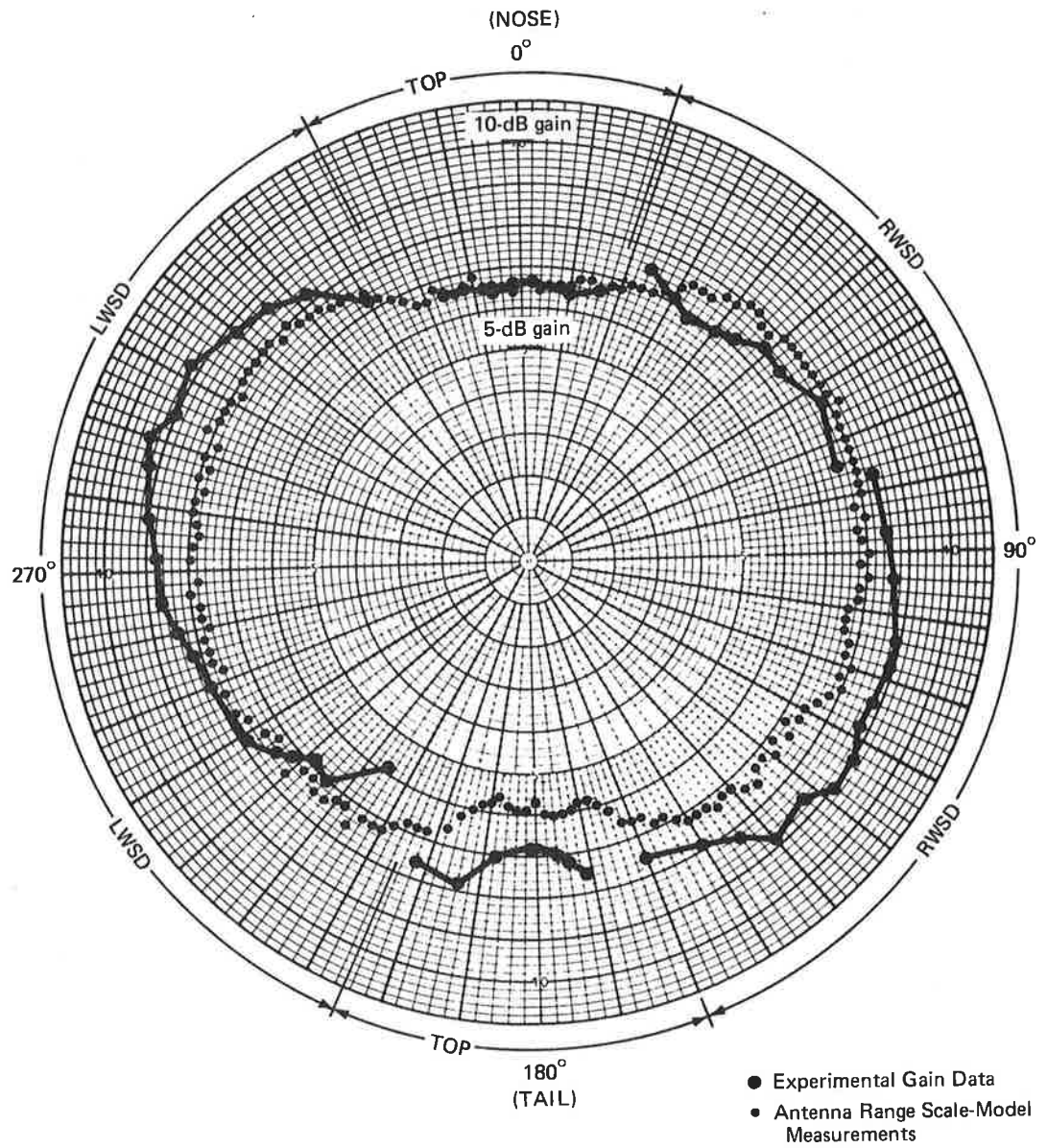


Figure 5-4. Slot-Dipole-System Composite Gain at 20° Elevation

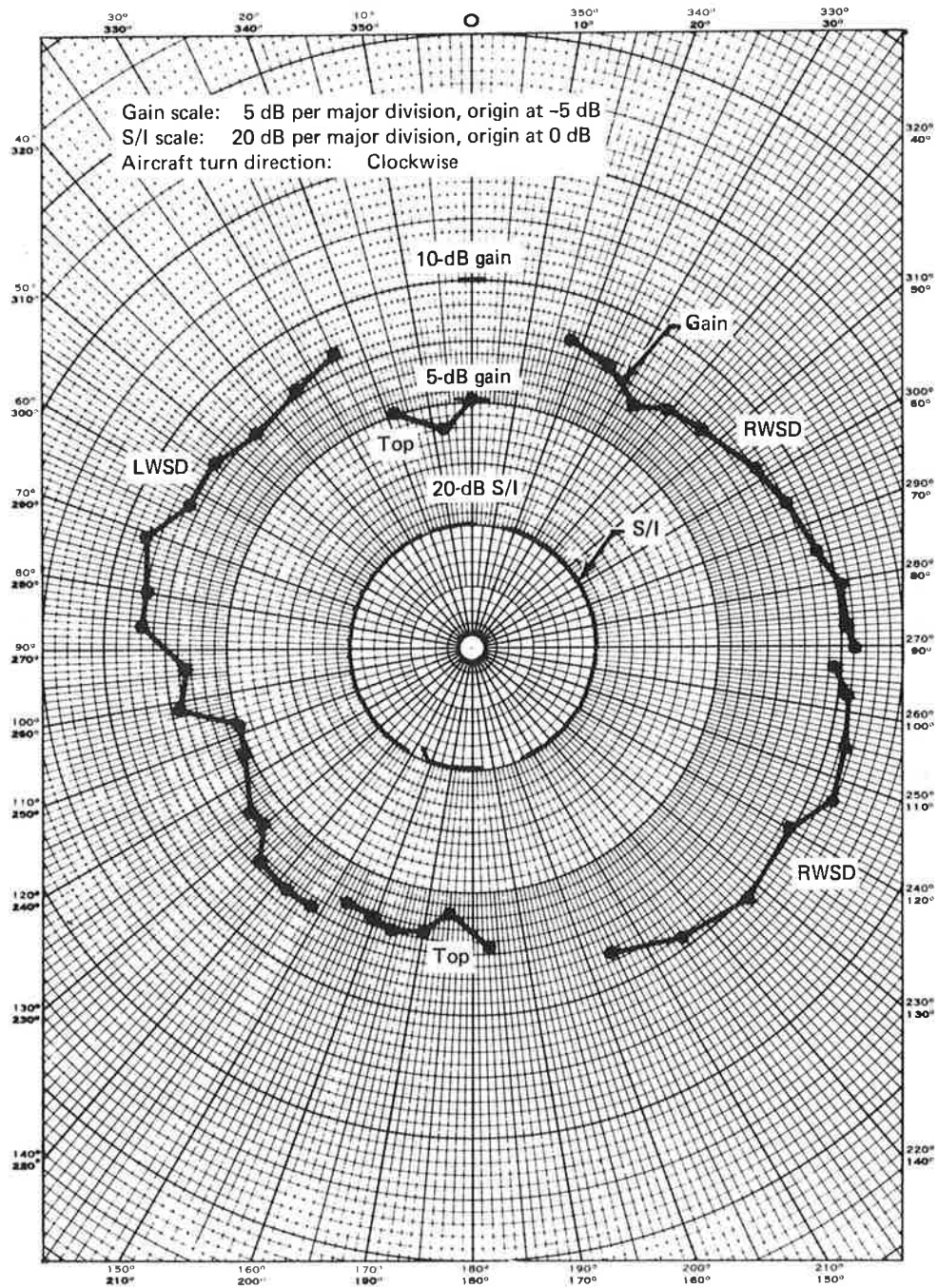


Figure 5-5. Three-Element Slot-Dipole Antenna System Gain and S/I, October 24, 1974, Elevation Angle = 19°

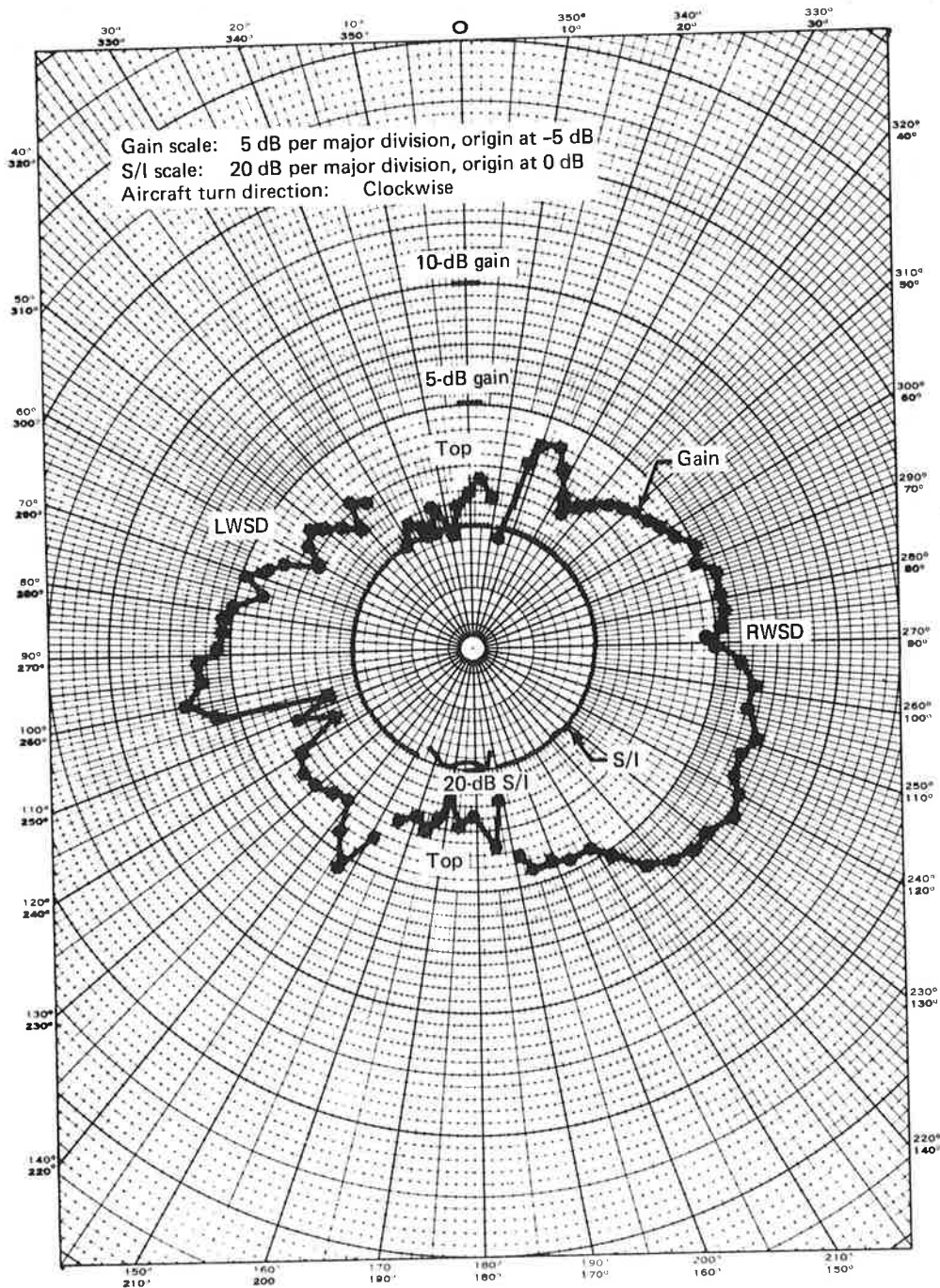


Figure 5-6. Three-Element Slot-Dipole Antenna System Gain and S/I, October 29, 1974, Elevation Angle = 16°

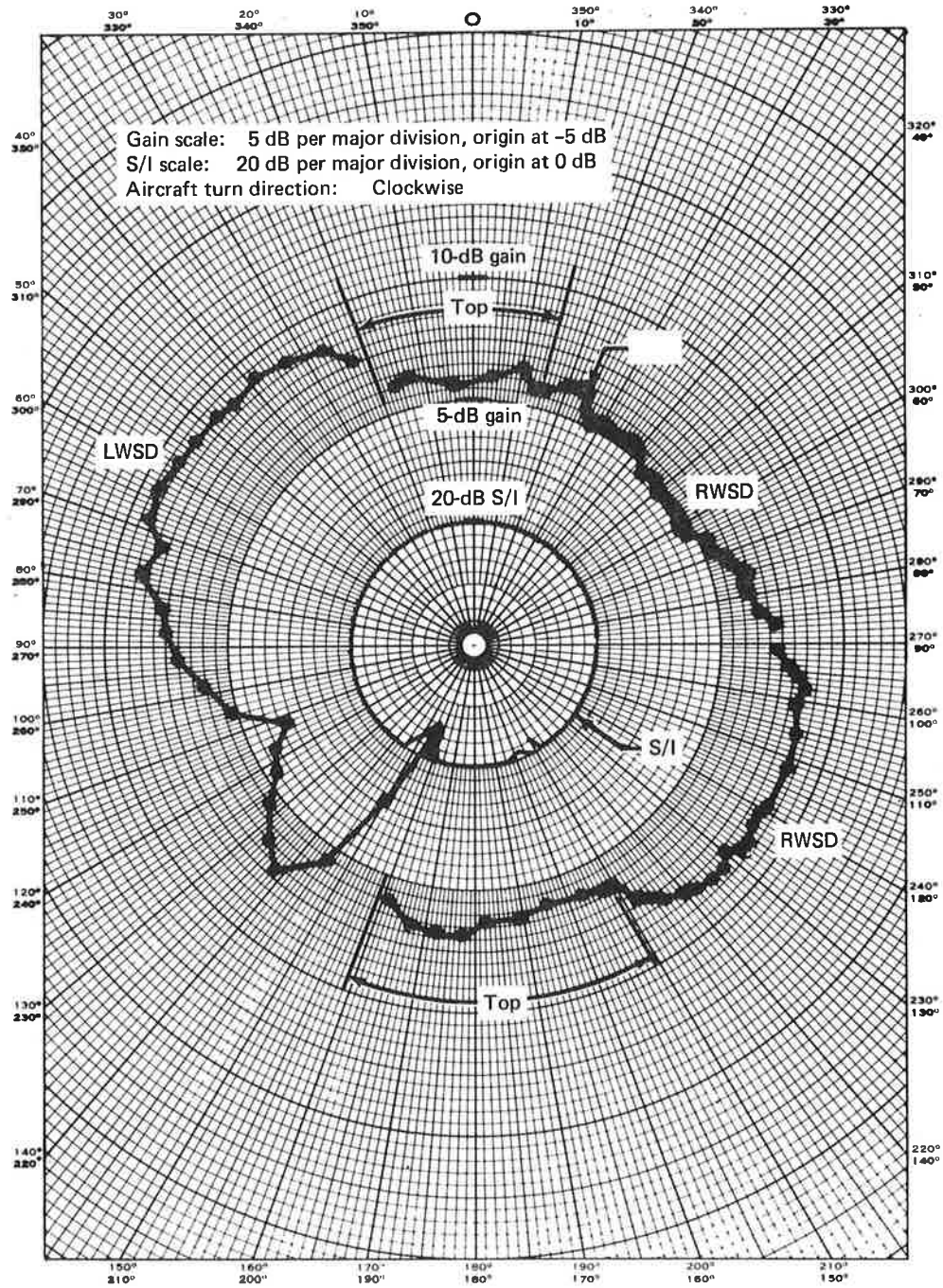


Figure 5-7. Three-Element Slot-Dipole Antenna System Gain and S/I, September 24, 1974, Elevation Angle = 28°

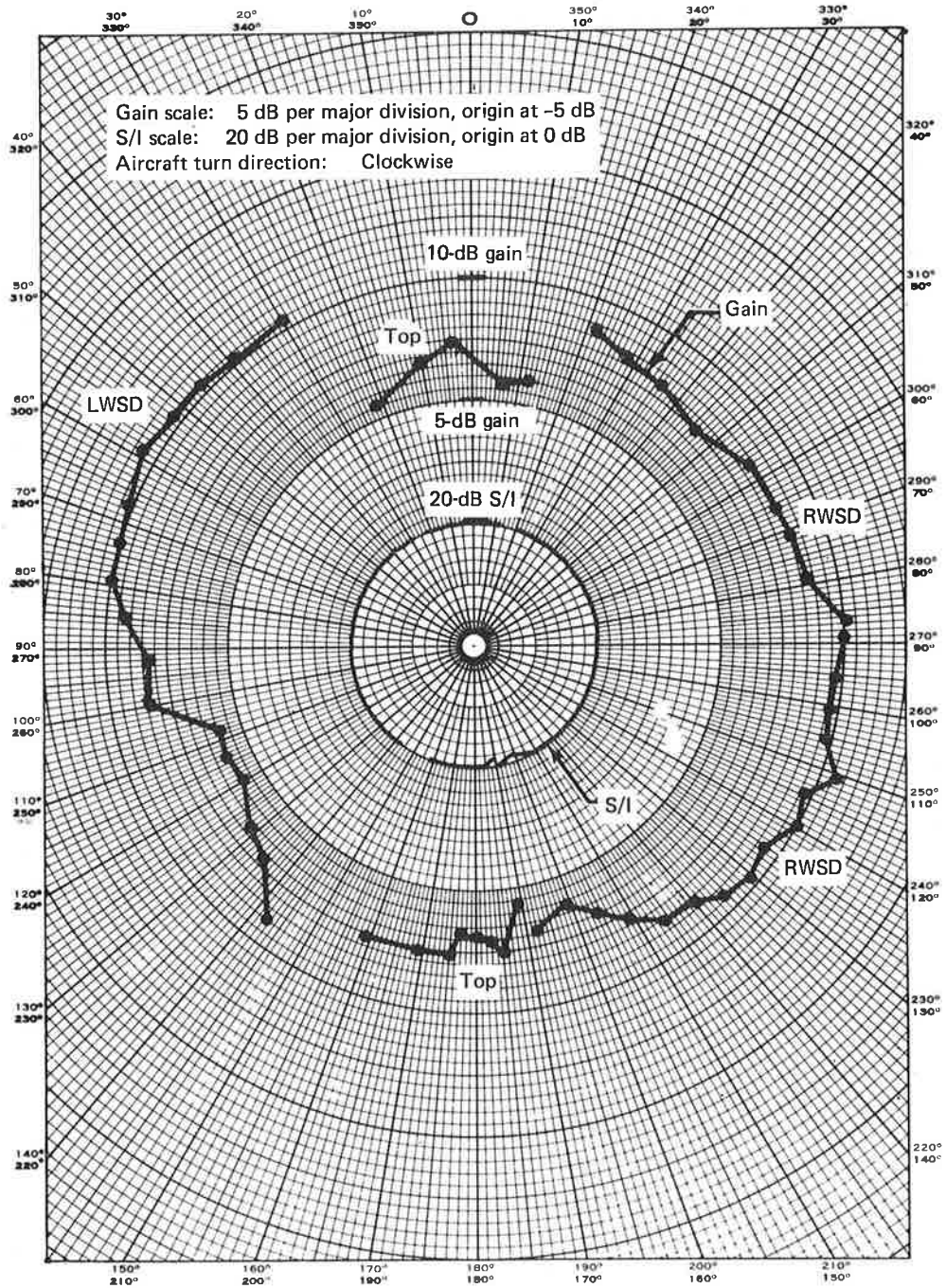


Figure 5-8. Three-Element Slot-Dipole Antenna System Gain and S/I, October 23, 1974, Elevation Angle = 25°

On April 1, the circular flightpath was counterclockwise as viewed from the top; i.e., the airplane heading was decreasing and the relative bearing to the satellite was gradually increasing during the test. The small bank angle for this circular path would be expected to effectively increase the elevation angle for the LWSD and decrease it for the RWSD. On this particular flight, westerly winds of approximately 150 kn were experienced at altitude. A discussion with flight personnel confirmed that a compensating banking maneuver would be expected, which would increase the effective elevation angle for the LWSD but would reduce the elevation angle during the RWSD illumination portion. As a result it is estimated that the broadside effective elevation angle for the LWSD is approximately 20° , while that for the RWSD is roughly 10° . At the lower elevation angles the antenna gain is very sensitive to small changes in elevation angle. The foregoing effects appear to explain the gain asymmetry in figure 5-1.

On March 25, the circular path was clockwise. The resultant bank angle would therefore be expected to have the opposite effect on effective elevation angle for the two side-mounted antennas (increase for RWSD, decrease for LWSD). Because wind velocity was less than on April 1, any compensating bank angle due to crosswind should be less for this test. Again, the effects of bank angle seem to be present in the data of figure 5-2. Comparison with figure 5-1 also reveals the complementary nature of the measured antenna gains, which is attributed to the opposite direction of circular flight for the two tests. The reason for the March 25 signal dropout at 10° left of the nose is not known (fig. 5-2). This type of dropout was not observed on any other data runs at similar geometries and hence it can be concluded that it is due to causes other than the antenna itself.

A third test result corresponding to an elevation angle of 19° is presented in figure 5-3. This test was conducted on November 21, 1974, with the circular portion being in a clockwise direction. The aircraft parameter data shows that the average bank angle was near 0° for the major portion of the test, with only a few excursions in excess of 5° . The pitch angle was in the range of 3° to 7° , nose-up attitude. The results agree reasonably well with the higher elevation angle portions of the March 25 and April 1 tests, but a higher than expected gain was observed for the RWSD between 90° and 160° from the nose. For the clockwise flightpath used, data for these angles was acquired on the northeast quadrant of the circle. The test area was near the 3-dB contour of the ATS-6 antenna pattern. Pattern overlays on the test area show that nonuniform illumination by the ATS-6 antenna of 1 to 2 dB is likely, with the maximum signal strength expected in the northeast quadrant. This may explain the unexpectedly large apparent gain for this portion of the test.

A composite-gain pattern derived from the foregoing three tests is shown in figure 5-4. The LWSD data is primarily taken from the April 1 test, the RWSD data is essentially that of the March 25 test, and the TOP data is a weighted combination of all three. This represents an experimental composite-gain conic for the slot-dipole system for an elevation angle of about 20° . For reference, the antenna range scale-model gain conic obtained from radiation distribution plots is given and is seen to agree reasonably well with the experimental data.

Figure 5-5 plots gain and S/I for the TOP/RWSD/LWSD system for the October 24, 1974, test at an elevation angle of 19°. Because of an intermittent RF switch, the QH antenna could not be connected and therefore, real-time QH gain calibration data could not be acquired during the test. Calibration of antenna gain therefore involved estimating the ATS-6 downlink signal power by means of extrapolation from C/N₀ measurements made during modem evaluation tests conducted during the same flight. The overall antenna gain shown in figure 5-5 is about 2 dB higher than the gains shown in figures 5-3 and 5-4 even though all three tests have the same nominal elevation angle. It is believed that the 2-dB gain discrepancy apparent in figure 5-5 results from underestimating the ATS-6 forward-link power.

Figure 5-6 plots gain and S/I for the TOP/RWSD/LWSD system for the October 29, 1974, test. The nominal elevation angle to ATS-6 was 16°. Examination of the aircraft parameter data (fig. 4-1) shows that roll angle varied by only roughly 2°. Figure 5-6, together with figures 5-1 and 5-2, illustrate the sensitivity of antenna gain to effective elevation angle at the lower elevation angles.

Figures 5-7 and 5-8 plot the results of the September 24 and October 23, 1974, tests at elevation angles of 28° and 25°, respectively. They can be considered as the high-elevation-angle antenna performance data. In general, they agree well with each other except for an overall gain difference of approximately 2 dB. This 2-dB discrepancy is believed to be due to calibration error in the gain reference data, which results in calculated gain values too low for the September 24 test. This observation is supported by data acquired while the aircraft was parked at NAFEC on January 21, 1975. During this parked test, various relative bearing angles were obtained by taxiing the aircraft to a new orientation between measurements. Results of this test, tabulated in table 5-2, agree closely with the results of the October 23 test.

**TABLE 5-2. RWSD ANTENNA GAIN DATA^a, JANUARY 21, 1975,
ELEVATION ANGLE = 40°**

Bearing angle to ATS-6, deg	Real-time measured C/N ₀ , dB-Hz	Antenna gain, dB
16	45.3	6.9
30	46.6	7.6
60	46.5	7.5
89	48.7	10.8
124	48.7	10.8 ^b
150	45.9	7.8 ^b
164	44.5	6.4 ^b

^aData acquired during KC-135 taxi test at NAFEC, Atlantic City, New Jersey.

^bDirect gain calibrator using quad helix was not available. ATS-6 forward-link calibration measurements made at other times and locations during the same test have been used.

Also shown in figures 5-1 through 5-8 (except fig. 5-4) are the measured values of S/I derived from computer analysis of the recorded envelope detector output. As previously mentioned in section 4, the S/I analysis procedure is capable of resolving S/I ratios up to values of 20 dB; therefore, points with calculated S/I values larger than 20 dB were plotted at the 20-dB level. For all cases it is observed that S/I is usually ≥ 20 dB, with occasional dips into the 15- to 20-dB range, and a few more severe drops in the vicinity of the nose for the top-mounted antenna. This S/I performance is in general agreement with predictions of S/I based on antenna range measurements used in conjunction with the specular-point and surface integration models discussed in the next section and the appendix. The high multipath rejection achieved is due in part to the fact that the wing-root location provides natural multipath shielding. The rather large S/I values observed are consistent with results for Type I digital data modem tests, where the BER curves closely resemble the performance predicted for a purely additive noise environment. The Type I BER curves thus confirm that S/I exceeded 15 dB.

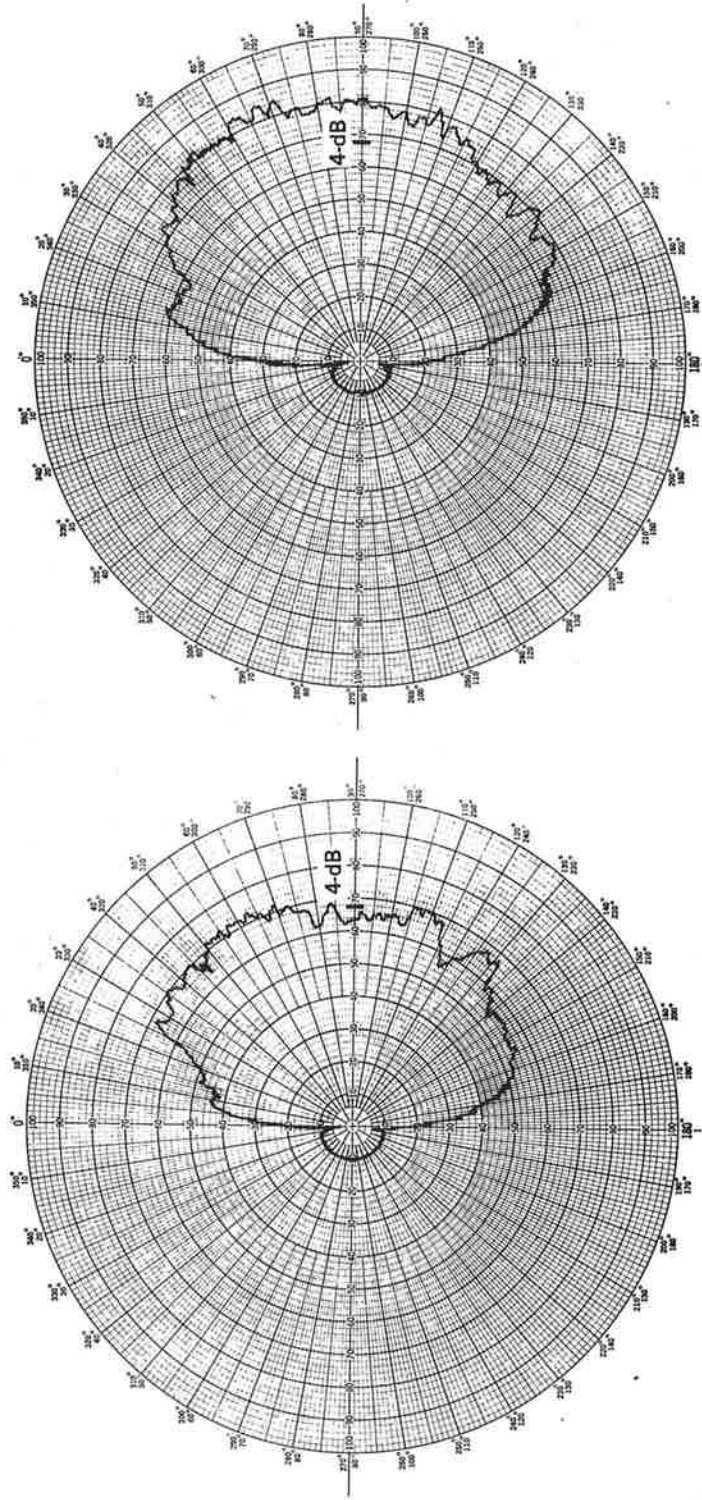
5.2 GAIN AND S/I DETERMINED FROM ANTENNA RANGE MEASUREMENTS

Principal-polarization and cross-polarization radiation patterns of the three-element slot-dipole system were obtained on an antenna range using scale-model antennas installed on a 1/20th-scale-model KC-135. For these scale-model measurements, the side-mounted antenna was installed at station 696 in the wing/body fairing area, a location somewhat forward of the actual installed location (station 766). These range measurements provided a full set of radiation distribution plots and analog gain patterns. The side-mounted antennas were sufficiently characterized to allow calculation of the theoretical S/I presented below.

Representative gain patterns (conics) from the scale-model measurements for one of the side-mounted antennas for angles of 10° , 20° , 30° , and 40° above the horizon are shown in figures 5-9 and 5-10. These figures are plotted in relative voltage units, with 67 V being equivalent to 4.0-dB gain.

A computer program was used in conjunction with the antenna range measurements to calculate the theoretical S/I ratio as a function of aircraft/satellite geometry for the side-mounted antennas. The top-mounted antenna was not included in these calculations because the range data acquired for the top antenna (RHC and LHC patterns) did not provide the complete antenna characterization required for the theoretical S/I calculations. The calculated theoretical S/I for the side-mounted wing-root slot dipoles is shown in figure 5-11. Although the S/I computations in the fore and aft directions are included, the TOP antenna would normally be used fore and aft. The S/I for the side antennas in these directions is therefore somewhat academic but provides a comparison reference for the experimental S/I data.

A rigorous determination of the multipath interference requires integration of the complex antenna pattern over the total ocean surface. In this derivation we have assumed the "steepest descent" solution and have characterized the multipath signal by its specular-point values. The results presented are thus



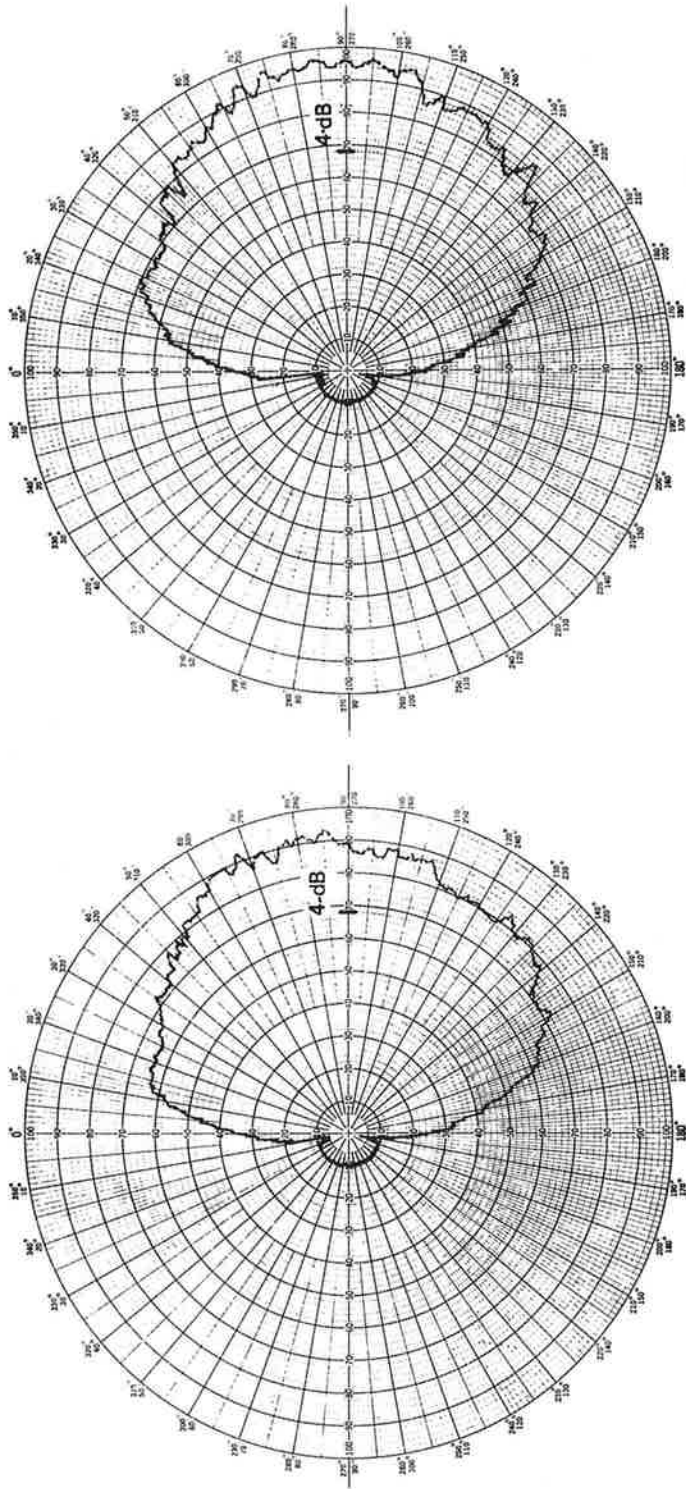
(a) Elevation Angle = 10°

(b) Elevation Angle = 20°

Note:

- 1) Plots are in voltage units, 67V equivalent to 4.0-dB gain.
- 2) Patterns are conical cuts; polarization is RHC.
- 3) Range data acquired using 1/20th-scale model

Figure 5-9. Wing-Root Slot-Dipole Antenna Range Gain at Elevation Angles of 10° and 20°



(a) Elevation Angle = 30°

(b) Elevation Angle = 40°

Note:

- 1) Plots are in voltage units, 67V equivalent to 4.0-dB gain.
- 2) Patterns are conical cuts; polarization is RHC.
- 3) Range data acquired using 1/20th-scale model.

Figure 5-10. Wing-Root Slot-Dipole Antenna Range Gain at Elevation Angles of 30° and 40°

not exact but are a good approximation, especially for modest sea-slope cases. In fact, the above approach may be argued to provide worst-case estimates of the antenna S/I parameter since the earth's divergence effect is neglected and the scattered energy is assumed to arrive only from the specular-point region. For grazing angles on the order of 10° , the divergence factor will attenuate the I component of the S/I by approximately 2 dB and if the aircraft antenna pattern is integrated over the diffuse sea scatter process, its well-known rolloff characteristics (θ -plane) provide further multipath rejection.

Some sample calculations of predicted S/I were made using an integration over the sea surface rather than the specular-point model. Because of the large amount of computer time required for the computation, only a few combinations of geometry and sea state were investigated. For the cases tested, a larger value of S/I was predicted by the surface integration model, as expected, providing good agreement with experimental data. Comparative results obtained for the specular-point and surface integration model are given in table 5-3. Details of the derivation of S/I from antenna range data are given in the appendix.

TABLE 5-3. COMPARISON OF SPECULAR-POINT AND SURFACE INTEGRATION MODEL PREDICTION OF S/I FOR SLOT-DIPOLE ANTENNA

Elevation angle, deg	Azimuthal angle, ϕ (from aircraft nose), deg	S/I predicted by specular-point model, dB	Surface integration model	
			RMS sea slope, deg	Predicted S/I, dB
15	90	17	9	22.0
19	45	20	1	23.6
19	45	20	6	25.0
19	45	20	15	26.8

5.3 DISCUSSION OF RESULTS AND CONCLUSIONS

Performance data for the three-element slot-dipole antenna system was acquired experimentally over a range of satellite elevation angles between 10° and 40° . At elevation angles above 20° , the experimentally measured three-element slot-dipole antenna system gain was in excess of 4 dB at essentially all azimuthal angles except in the forward direction with the TOP antenna. In the forward direction ($\pm 20^{\circ}$ from the nose), the TOP antenna gain was 3.5 dB for an elevation angle of 20° . The peak gain measured for the side-mounted antennas was approximately 10 dB. At the higher elevation angles, the experimentally measured gain frequently exceeded the gain values determined from antenna range data by about 2 dB.

Note:

- 1) S/I values computed in accordance with specular point model of the appendix. Values are in dB.
- 2) Conic angle $(\theta) = 80^\circ$ corresponds to elevation angle of 10° .
- 3) Slot-dipole antennas located at station 696 in wing-body fairing.
- 4) Range pattern data acquired using 1/20th-scale model.

Conic angle, θ	50	9	10	11	11	13	13	14	14	15	17	17	18	18	18	18	18	19	19	20	20	19	20	19
	8	9	10	12	12	13	15	14	15	16	17	17	17	18	18	18	18	19	19	19	19	19	19	20
	8	10	10	10	12	14	14	15	16	17	16	17	17	18	18	18	19	20	19	19	20	19	19	19
	9	8	11	12	12	15	14	15	16	16	16	18	18	19	18	18	19	18	19	18	19	18	19	19
	8	9	11	11	12	13	14	14	15	16	17	17	17	18	19	18	18	19	19	19	19	19	19	19
	60	8	10	11	13	13	14	14	15	16	16	18	17	19	18	18	19	19	18	18	18	19	19	20
	9	10	12	13	13	13	15	16	16	16	17	17	18	18	18	18	18	19	18	18	19	19	19	
	6	9	11	12	13	15	15	17	16	19	19	17	18	18	19	20	19	19	19	18	18	19	19	
	7	7	11	11	11	13	15	15	16	17	17	18	17	17	17	17	18	18	18	18	19	19	19	
	5	8	12	11	12	13	15	15	15	16	16	17	18	16	18	18	17	18	17	18	17	21	19	18
	70	6	7	9	10	12	12	14	15	16	19	16	17	17	17	17	17	17	17	18	18	17	18	18
	7	7	11	11	13	14	14	15	16	16	16	17	20	20	18	17	17	19	20	17	19	17	17	
	6	8	8	12	13	13	18	15	15	19	17	17	16	17	19	16	17	18	20	20	18	17	20	
	1	6	8	12	13	13	16	19	16	16	17	17	16	17	18	18	17	18	18	17	18	20	17	16
	4	8	8	12	14	14	15	17	17	17	18	16	17	17	17	16	17	20	16	18	16	16	16	
	80	0	5	10	12	14	16	15	18	18	19	17	18	17	17	17	19	16	18	17	17	16	19	15
	180		190		200		210		220															
	Azimuth angle, ϕ																							

Conic angle, θ	50	21	22	21	21	21	21	21	21	21	21	21	21	20	22	20	21	20	20	20	20	21	19	
	21	20	20	21	21	22	21	21	21	21	21	21	21	21	21	21	21	20	21	20	20	20	20	
	21	22	22	22	22	20	20	21	20	21	21	21	20	21	21	21	20	21	20	21	20	21	19	
	20	20	21	21	21	21	20	20	22	21	21	21	21	21	21	20	20	20	19	20	21	19	19	
	22	20	22	21	20	21	21	22	20	22	21	22	21	21	21	21	21	21	20	21	21	19	19	
	60	20	21	20	21	22	22	21	21	21	20	21	20	22	22	23	22	22	20	20	20	19	20	
	21	20	20	20	21	21	20	20	20	20	21	20	20	20	22	21	21	21	21	20	21	19	19	
	20	19	22	20	20	19	20	20	20	19	20	20	20	21	20	20	21	20	22	20	19	19	19	
	19	20	19	19	19	19	19	19	20	21	21	20	20	20	20	23	21	21	21	20	20	21	21	
	19	19	18	18	20	19	21	19	20	20	20	21	21	20	20	20	20	20	20	20	20	20	19	
	70	18	18	20	19	19	19	18	19	19	19	20	20	21	20	19	20	20	20	21	20	22	20	
	18	19	19	21	19	19	18	21	19	20	19	19	20	20	19	20	20	19	20	19	20	19	20	
	19	18	17	18	18	21	19	19	18	19	20	20	20	21	21	19	20	20	21	20	22	20	21	
	17	18	18	18	17	19	18	18	21	19	20	22	21	20	20	20	20	20	22	20	22	20	21	
	16	16	17	18	17	16	17	17	18	19	21	18	18	18	19	23	20	21	20	18	18	19	18	
	17	16	17	16	17	17	16	17	17	19	18	16	16	16	20	17	17	17	17	16	17	16	16	
	270		280		290		300		310															
	Azimuth angle, ϕ																							

21	20	20	20	20	21	20	21	21	20	21	21	20	21	21	21	21	22	21	21	21	21	21	50
20	19	20	20	21	20	20	20	20	21	21	21	21	21	21	21	21	22	21	21	21	22	21	21
20	20	20	20	20	20	22	20	21	20	20	21	20	22	21	21	21	21	21	20	21	20	21	21
20	20	19	19	19	20	20	20	20	20	21	21	21	21	21	21	20	22	21	20	20	21	20	20
19	20	19	19	19	20	19	20	21	19	19	20	20	20	20	20	20	20	21	20	20	20	21	22
19	20	20	20	20	21	20	19	19	20	21	19	20	21	21	21	22	21	21	21	20	20	20	20
18	19	19	20	19	19	20	19	20	19	20	20	21	21	21	22	21	21	21	21	20	20	20	21
18	20	19	18	19	20	21	19	19	20	19	19	19	19	19	20	21	20	20	20	20	21	18	20
18	18	19	19	18	18	18	19	19	20	20	18	20	19	19	19	19	19	20	19	19	19	20	19
18	18	18	18	18	18	18	20	20	19	19	19	19	19	19	19	19	19	19	19	19	20	20	19
17	17	17	18	18	18	18	19	18	18	19	20	19	18	19	18	19	18	19	19	18	19	20	19
18	18	21	18	18	18	18	18	18	20	19	18	18	19	18	20	21	18	18	19	20	19	18	18
17	17	17	17	17	18	17	17	18	18	18	18	18	18	18	19	18	17	17	19	18	19	17	18
16	17	18	15	18	16	16	16	16	16	16	16	16	17	16	16	18	18	18	18	20	18	17	17
16	15	16	16	18	16	15	17	17	18	18	17	19	17	15	17	16	17	17	16	17	16	17	16
16	17	17	16	17	19	18	18	15	14	15	19	18	17	17	17	17	17	17	17	16	16	17	80
		230				240						250					260					270	
Azimuth angle, ϕ																							

20	20	20	19	19	19	18	19	18	18	19	18	18	18	18	18	17	17	17	15	16	15	50
19	19	19	19	19	19	18	18	19	18	18	19	18	18	18	18	19	17	17	17	16	15	15
19	19	18	19	19	20	18	19	18	18	18	18	18	18	18	18	18	17	17	17	16	15	14
19	19	19	19	19	19	18	18	19	18	18	18	18	18	18	18	18	18	17	16	15	15	15
19	18	20	19	19	20	18	19	19	19	18	18	18	18	18	18	18	18	17	16	15	16	14
19	19	19	20	19	19	18	18	20	18	18	18	18	18	18	18	17	18	17	16	15	14	60
20	21	19	19	19	20	19	19	19	19	18	17	17	17	18	18	17	17	18	16	16	15	15
21	19	20	19	21	20	19	21	20	20	18	18	17	18	18	18	17	17	16	16	16	16	16
19	19	19	19	21	20	20	21	21	19	19	18	18	18	20	18	17	17	17	16	16	15	14
20	20	21	21	20	22	20	21	21	19	21	19	19	19	20	20	19	17	16	16	15	15	15
21	20	21	21	22	21	21	20	21	21	20	21	20	19	18	17	20	19	19	19	16	15	15
20	22	21	22	22	20	20	20	21	20	19	18	17	20	18	19	19	20	19	18	18	15	70
21	22	21	20	20	20	21	20	21	22	21	19	18	17	17	19	17	20	19	17	17	15	15
22	22	21	20	18	17	17	16	18	18	18	22	20	17	20	20	17	18	18	15	17	15	15
18	19	20	17	16	16	16	15	15	16	16	17	17	16	16	17	18	18	18	15	17	14	14
16	16	15	14	14	15	14	13	14	14	14	14	14	14	13	14	16	15	16	17	16	14	12
		320				330							340				350					360
Azimuth angle, ϕ																						

At elevation angles below 20° , the experimental gain measurements were quite sensitive to aircraft motions affecting the aircraft/satellite geometry but were in general agreement with range data gain values. Although experimental scatter was observed in the measured gain data, there was no evidence of significant pattern holes or coverage deficiencies at any of the geometries tested. The several sets of data at a nominal elevation angle of about 15° illustrate that gain measurement repeatability at low elevation angles is difficult because of the sensitivity to aircraft maneuvers caused by the characteristic rapid change in gain patterns at the lower elevation angles.

The experimental data suggests that the slot dipoles may be somewhat more directional in the roll plane than indicated by the range data. If the antenna directivity was in fact higher than indicated by the range data, gain values lower than expected would necessarily occur at some other geometry, presumably at the lower elevation angles. Although sensitivity to aircraft motions was observed at the lower elevation angles, the experimental scatter of the data and the relatively small amount of data available preclude drawing firm conclusions on this point.

Specific items with potential for causing the experimentally measured gains to exceed those determined from antenna range measurements have been investigated but have not been positively isolated as contributors. Several possibilities are discussed below.

- a. The overall RF insertion losses (L_t in table 4-1) have an uncertainty (in all cases less than 1.0 dB) since the antenna transmission lines and the RF control units were calibrated separately because of experimental necessity. The total insertion loss was computed as the sum of these contributions and included an estimated allowance for the short interconnecting cables and mismatch at the interconnection ports. Review of available calibration data suggests that the value of L_t tabulated for the RWSD and LWSD RF paths may be too large by 0.5 to 1.0 dB. This observation is supported by the small discrepancy between the value of NF_{opm} and NF_{ope} tabulated for the RWSD and LWSD in table 4-1. As shown by equations (4-1) to (4-3), an error in L_t translates directly into a corresponding error in the calculated antenna gain. It is therefore possible that calculated gains for the RWSD and LWSD are too large by 0.5 to 1.0 dB due to this contribution. (Error contribution due to NF_{op} measurements is believed to be small because of the high degree of consistency indicated by the cross-checks available and the large number of measurement repetitions.)
- b. The antenna gain values calculated from the experimental data would contain a systematic error, making the values too high, if the actual in-flight gain achieved with the quad-helix reference antenna was less than the 15.5-dB value determined from full-scale measurements on the antenna change. It is believed that systematic error caused by overestimating the gain of the reference antenna is less than 0.5 dB since (1) experimentally measured peak gains of the phased array and patch agree well with expected values, thus supporting the 15.5-dB reference gain used and (2) the quad-helix antenna was removed and recalibrated on the antenna range on two separate occasions, each time confirming the 15.5-dB value employed. It should also be noted that any systematic error in the gain value assumed for

the quad-helix reference-gain antenna will affect the calculated gains for all antennas (slot dipoles, phased array, patch) identically. Gain data for these antennas relative to each other would therefore be unaffected by an error of this type.

- c. The scale-model patterns of the slot-dipole antenna were taken at station 696, whereas the antennas were actually installed at station 766 of the KC-135 because of insufficient space at the original design location. This relocation of the antennas is believed to have small effect on the patterns at elevation angles above 10° and, in particular, should not influence the peak gain. This factor is therefore believed to be only a minor contributor, if at all, to the higher than expected gains observed.

The experimentally measured gain of the TOP antenna was usually observed to be less in the forward than in the aft direction, indicating that the normal aircraft pitch angles (4° to 6° nose-up) may be influencing performance. This suggests that a more forward location of the TOP antenna might result in improved over-the-nose performance at low elevation angles.

The experimental data showed conclusively that very good multipath rejection was achieved by the three-element slot-dipole antenna system at all geometries tested. The S/I was usually greater than 20 dB, with occasional dips into the 15- to 20-dB range, and a few more severe drops in the vicinity of the nose for the top-mounted antenna. This performance is in general agreement with the predicted S/I values based on antenna range measurements. The rather large S/I values observed are consistent with results for Type I digital data modem tests, where the bit-error-rate (BER) performance curves closely resemble the performance predicted for a purely additive noise environment without multipath interference. The Type I BER curves thus confirm that S/I exceeded 15 dB.

6. PHASED-ARRAY ANTENNA TEST RESULTS

This section presents plotted and tabular gain and S/I data for the phased-array antenna.

6.1 EXPERIMENTAL GAIN AND S/I DATA

One portion of the phased-array antenna data was acquired from the "straight-line" flight segments as described in section 3.3. Test results are presented in table 6-1 and figure 6-1. Three groups of data were collected on the following dates and locations:

- a. Ground test at NAFEC on January 21, 1975, at an elevation angle of 40°
- b. Flight test on March 27, 1975, over the North Atlantic at elevation angles between 10° and 15°
- c. Flight test on January 27, 1975, over the North Atlantic at elevation angles between 15° and 18° .

During each straight-line segment, the optimum beam position for maximum signal reception was experimentally selected. The beam positions are identified in table 6-1 according to the manufacturer's nomenclature. Since quad-helix gain calibration data is not available for all straightline segments, the phased-array gain values sometimes use signal strength calibration measurements of the ATS-6 downlink that were made at other times or locations during the same test. These cases have been identified by footnote a in table 6-1.

Five tests were also conducted on normal circular-track antenna flights and are plotted in figures 6-2 through 6-6. A summary of test conditions is tabulated in table 6-2. Due to the antenna's location, data could be acquired only in the right-hand hemisphere.

For the test of September 24, 1974, at 28° elevation, the elevation beam position selected resulted in near-optimum reception throughout the flights. The data values plotted in figure 6-2, however, appear to be about 1 dB below their expected true values, possibly due to a calibration error for this test. The concurrent RWSD data plotted in figure 5-7 also indicates this possibility.

From the results achieved on the September 24, October 29 (fig. 6-3), and straight-line segment tests, it is observed that when the elevation beam position is optimized, the array provides gain of about 10 to 12 dB over a broadside sector. As the azimuth changes toward 0° or 180° , the gain decreases as expected. The measured S/I for this antenna was always in excess of 20 dB whenever the beam position was optimized. This appears to be the expected result due to the narrow roll-plane beamwidth and the side-lobe taper control.

TABLE 6-1. PHASED-ARRAY GAIN DATA FOR LINEAR FLIGHTPATHS

ATS-6 direction, deg		Optimum antenna beam position	C/N ₀ , dB-Hz		Received signal level, -dBW	Antenna gain, dB
Relative bearing	Elev		Real-time measured	Computer analyzed		
NAFEC Ground Test, January 21, 1975						
16	40	7	42.9	N/A	149.8	5.5
30	40	6	45.1	N/A	147.6	6.8
60	40	5	47.2	N/A	145.5	8.9
89	40	4	48.0	N/A	144.7	10.8
124	40	5	48.1	N/A	144.6	10.9
150	40	6	45.7	N/A	147.0	8.5 ^a
164	40	7	42.1	N/A	150.6	4.5 ^a
Flight Test, March 27, 1975						
26	12	3	46.6	45.0	147.7	4.3
55	11	2	48.5	46.4	146.3	5.5
82	10	1	50.0	49.9	142.8	9.4
111	11	2	46.0	45.4	147.3	4.5 ^a
147	12	4	43.2	42.5	150.2	1.8 ^a
Flight Test, January 27, 1975						
18	16	4	41.4	41.6	151.1	4.4 ^a
44	17	2	42.9	42.7	150.0	8.7
78	18	2	49.2	49.0	143.7	9.3
111	17	2	51.8	51.5	141.2	11.3 ^a
145	16	3	47.9	47.6	145.1	7.4 ^a

^aIndicates that direct gain calibration using the quad helix was not available. ATS-6 downlink calibration measurements made at other times and locations during the same test have been used.

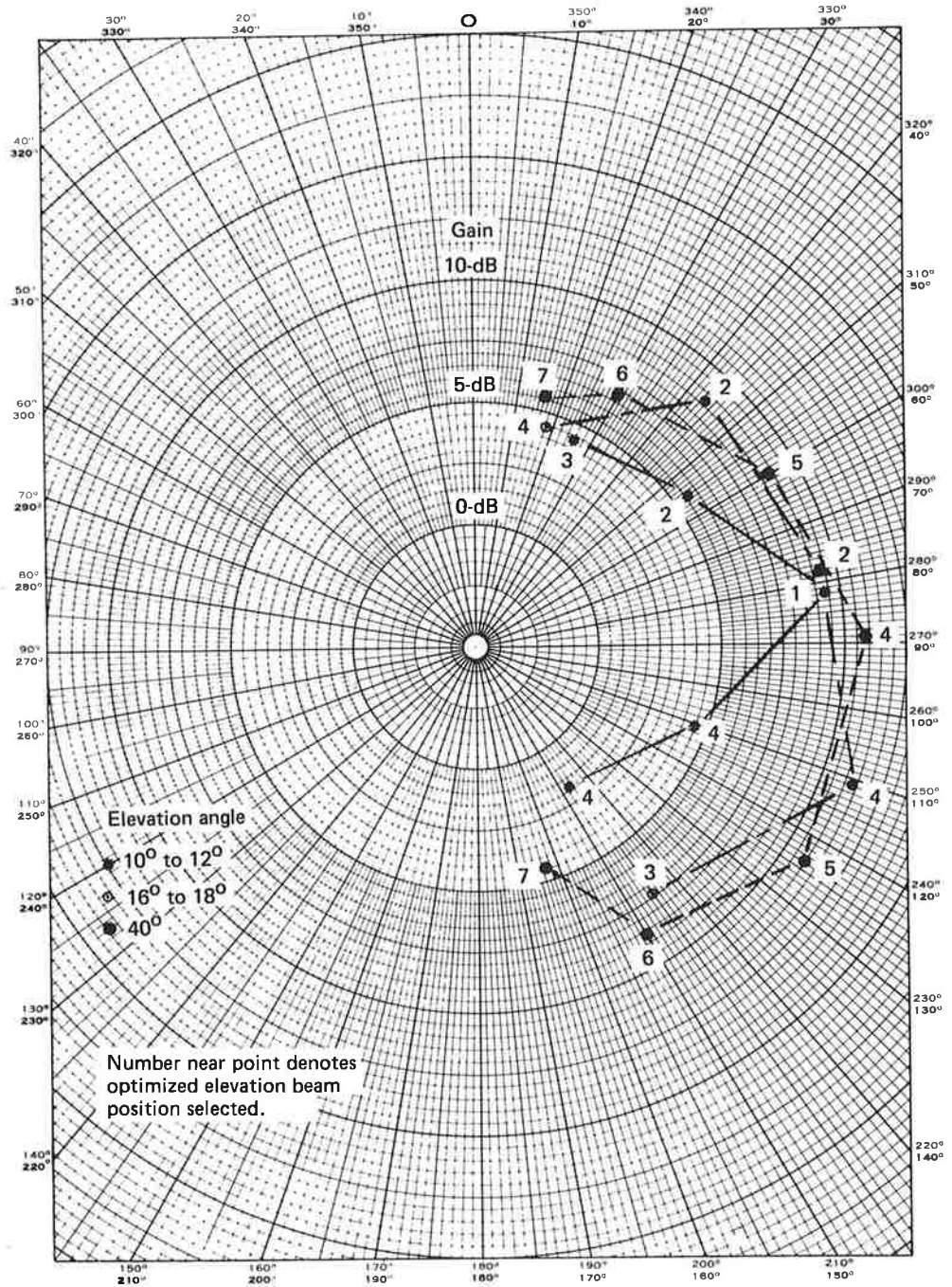


Figure 6-1. Phased-Array Gain Data for "Straight-Line" Tests

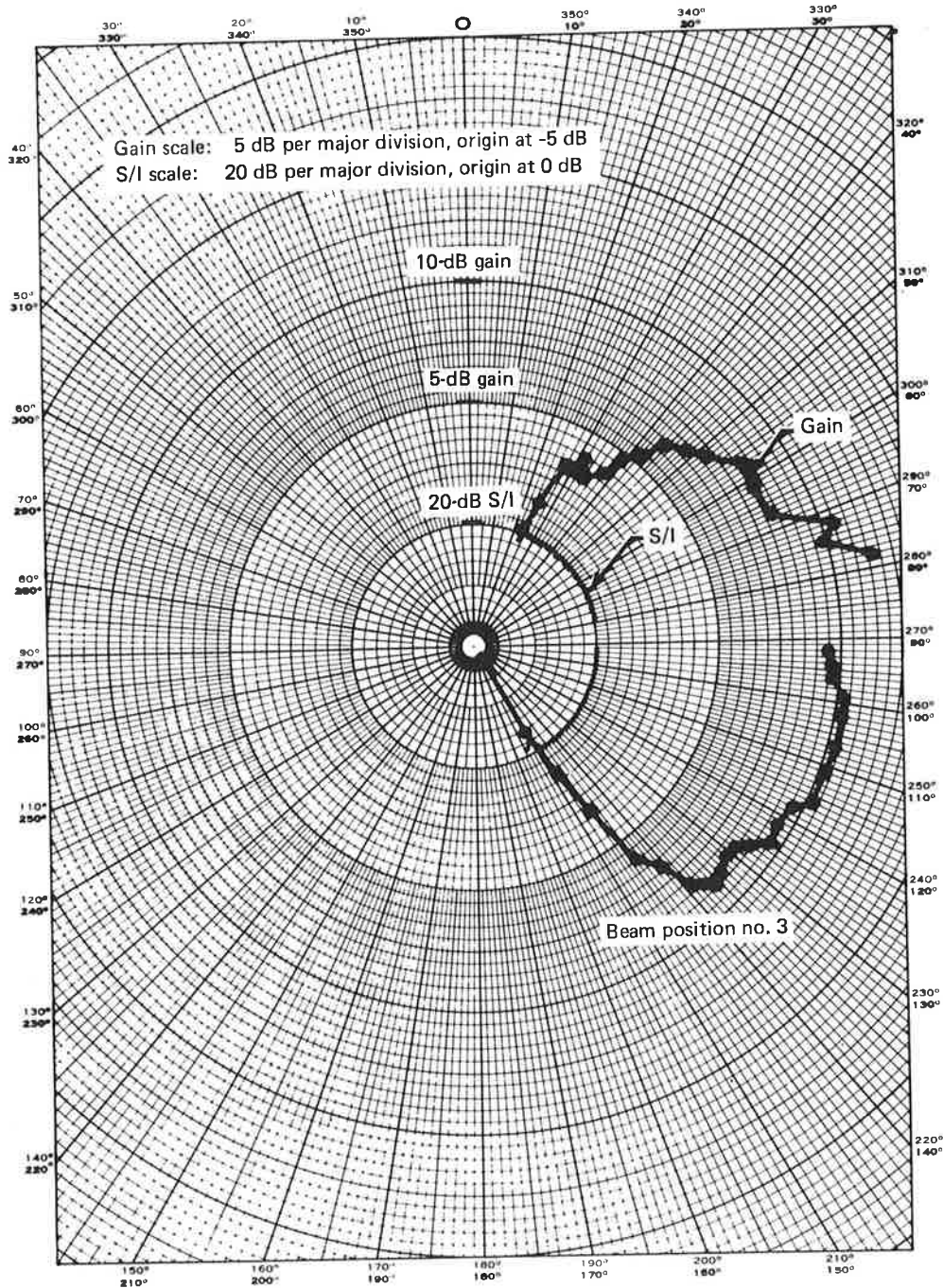


Figure 6-2. Phased-Array Antenna Gain and S/I, September 24, 1974, Elevation Angle = 28°

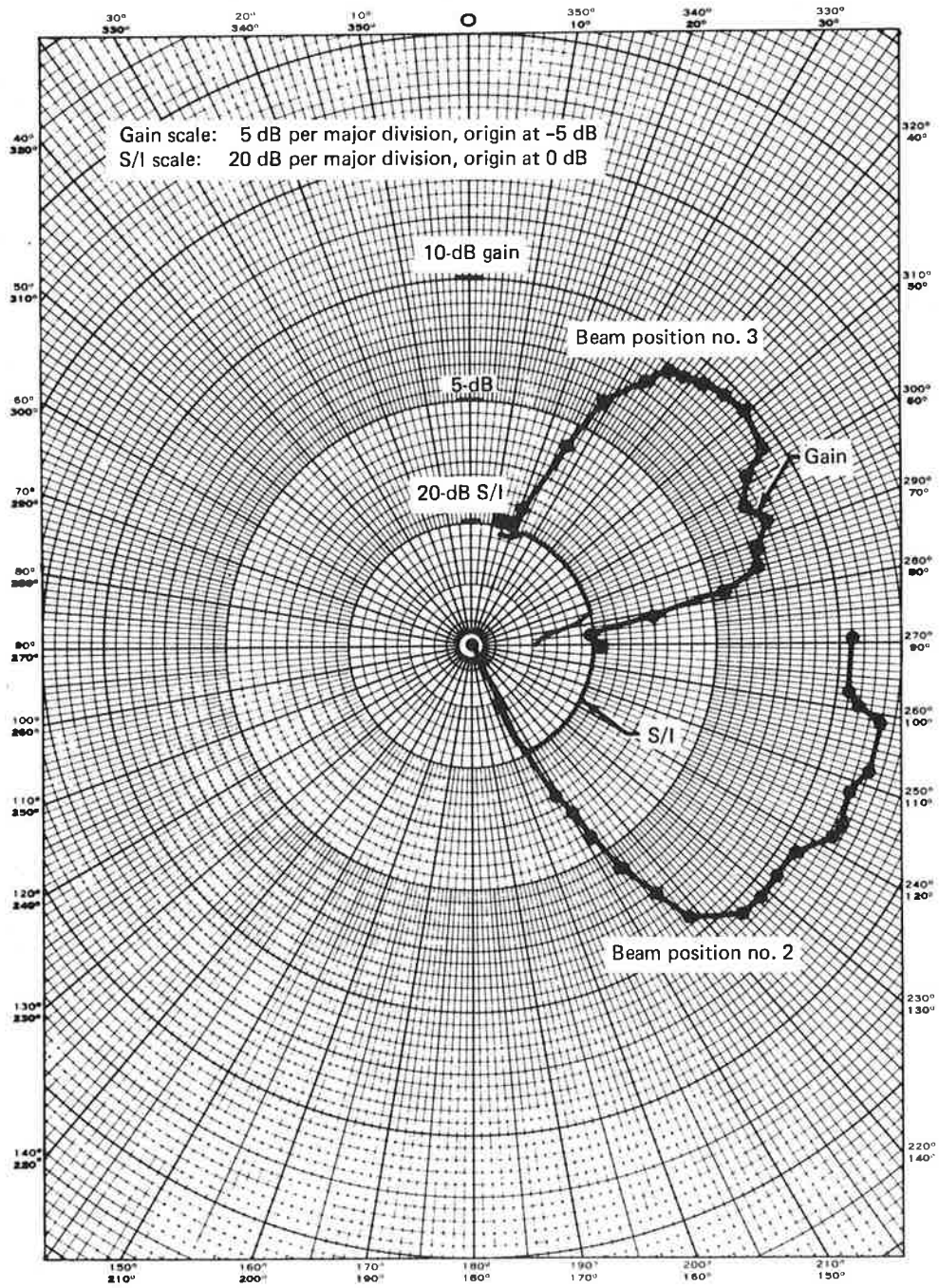


Figure 6-3. Phased-Array Antenna Gain and S/I, October 29, 1974, Elevation Angle = 16°

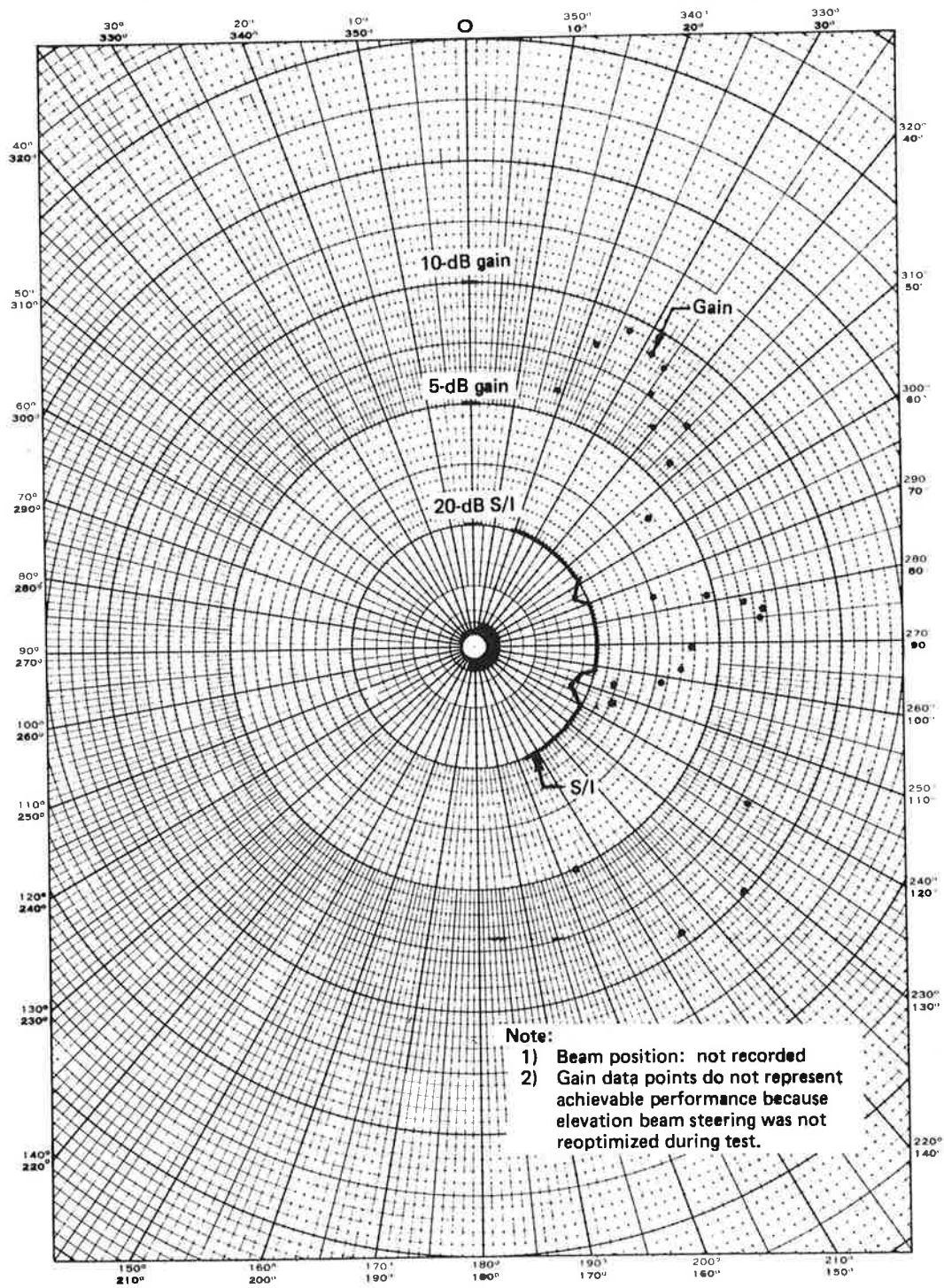


Figure 6-4. Phased-Array Antenna Gain and S/I, October 24, 1974, Elevation Angle = 19°

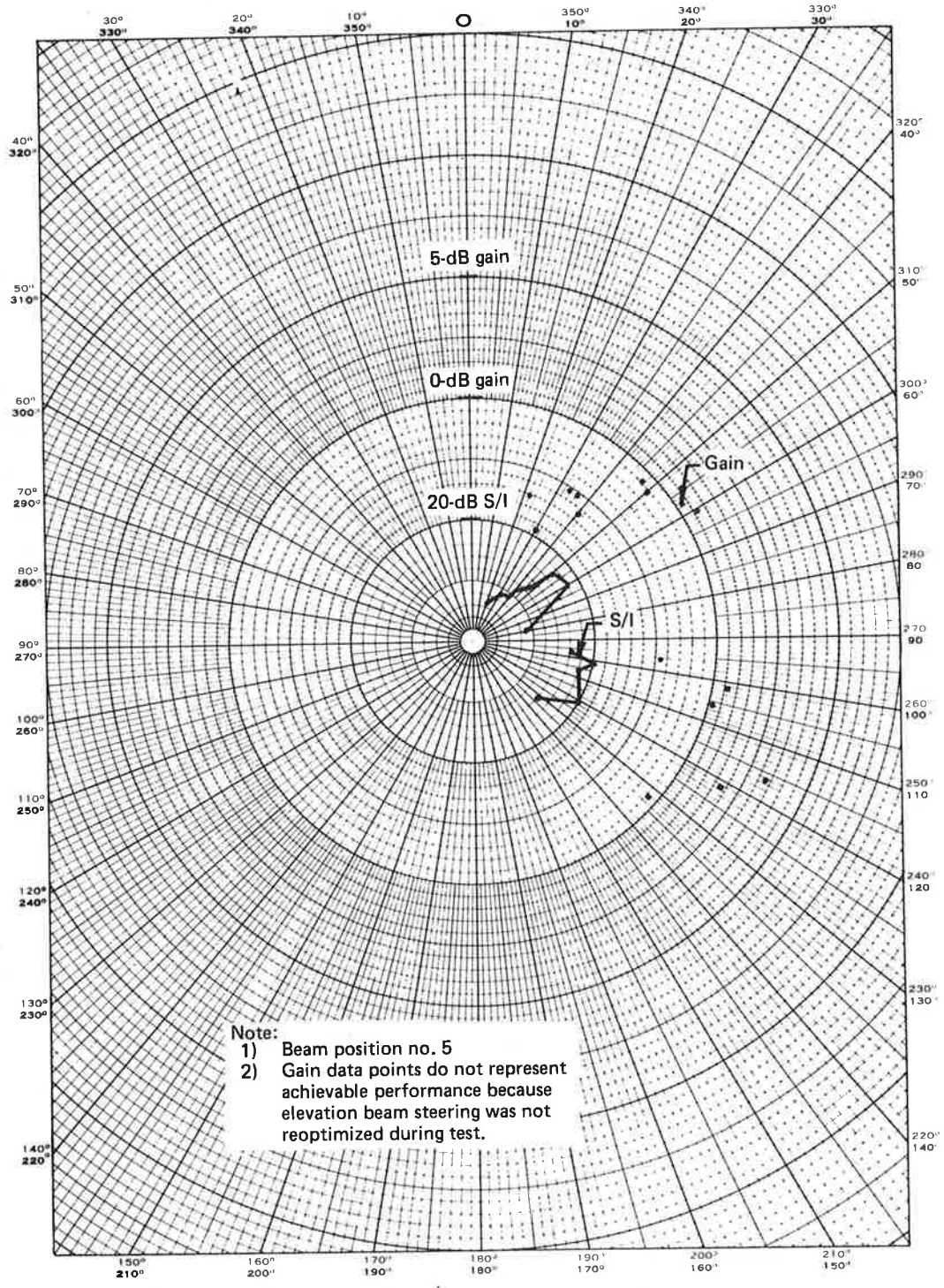


Figure 6-5. Phased-Array Antenna Gain and S/I, November 21, 1974, Elevation Angle = 19°

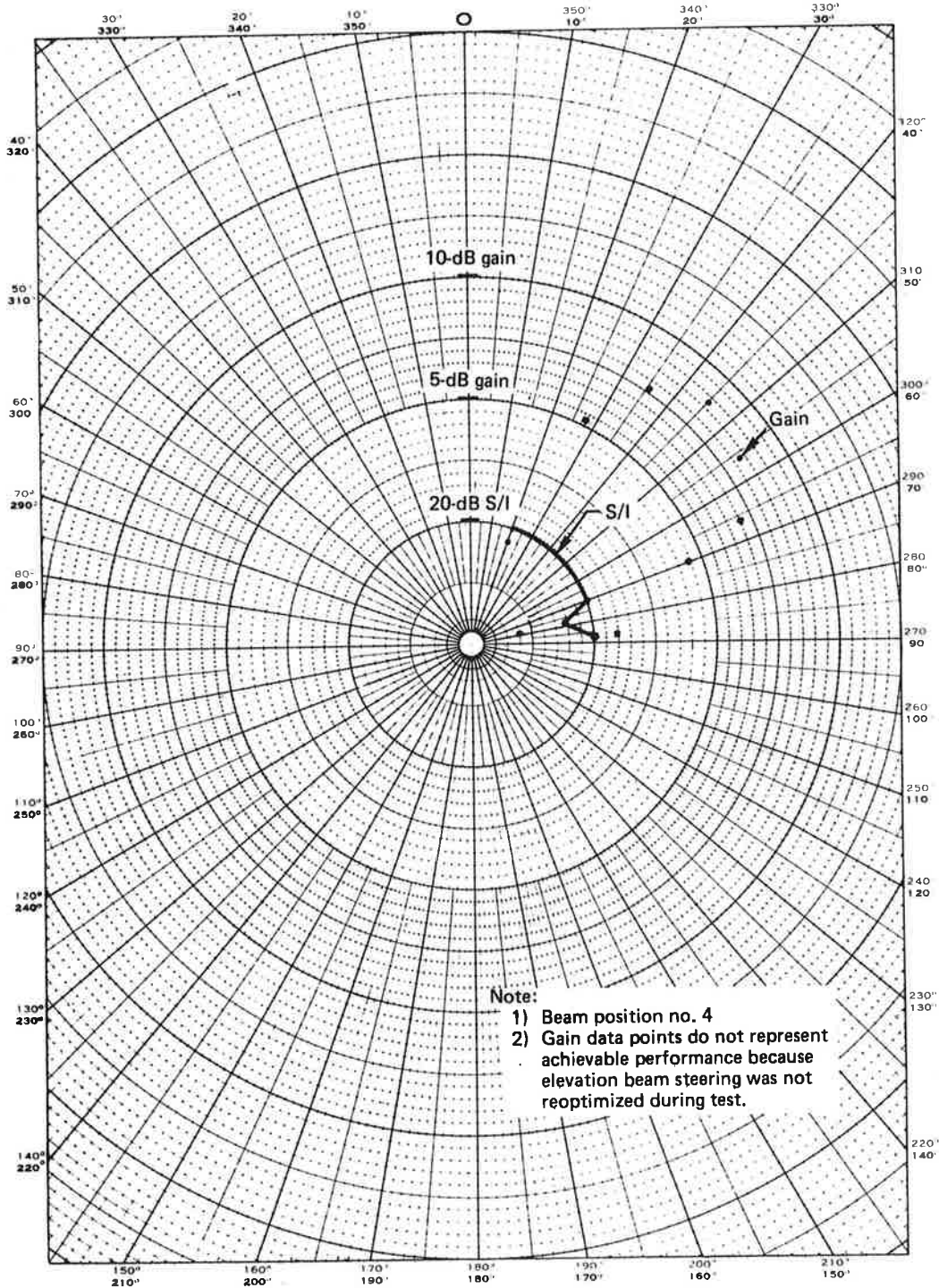


Figure 6-6. Phased-Array Antenna Gain and S/I, October 23, 1974, Elevation Angle = 25°

Experimental data for other circular flights are provided in figures 6-4 through 6-6. For these flights, the elevation beam position selected prior to the start of the test did not provide optimum reception throughout. These experimental data therefore do not represent the achievable performance under optimized conditions and thus are of rather limited value. However, the data do illustrate, to some degree, the two response peaks separated by reduced gain directly broadside. This is the typical gain pattern obtained when a conical cut is made through a single characteristically shaped beam of the phased-array antenna. The response peak at $\phi = 85^\circ$ in figure 6-4 is unexpected and the reason for its appearance is not known. The interdependency of optimum elevation beam position and relative bearing angle are also indicated in table 6-1.

Circular and straight-line flight test data show that the phased array, as mounted on the KC-135, provided a peak gain of 11 to 12 dB approximately broadside at an elevation angle of 40° . This measured value agrees well with the full-scale antenna range peak gain value. At an elevation angle of 40° , the 3-dB azimuthal beamwidth was approximately 100° , providing coverage between 50° and 150° from the nose. From the small amount of data available at elevation angles of 10° , the experimentally measured maximum achievable gain was between 9.0 to 9.5 dB and 3-dB azimuthal beamwidth was approximately 50° . At azimuthal angles beyond the above useful coverage region, the gain dropped rapidly to low or negative values. No attempt was made to measure side-lobe levels experimentally.

The antenna exhibited consistently good multipath rejection, with the measured S/I being in excess of 20 dB within the useful coverage region.

6.2 ANTENNA RANGE PATTERN MEASUREMENTS

Radiation pattern measurements were made by the antenna manufacturer, Ball Brothers Research Corp. Range patterns taken with the full-scale antenna mounted on a 4-ft ground plane show that expected peak gain is approximately 12 dB and roll-plane beamwidth is between 12° and 15° for each of the nine selectable elevation beam portions.

A limited number of scale-model pattern measurements were also made by the manufacturer. One-tenth-scale antenna units were designed for beam positions 1, 2, and 4. Beam positions 1 and 2 were selected since they are most likely to be affected by the presence of the aircraft wings. Beam position 4 was selected since it represents the higher steering angles and would allow comparison of the patterns from the full-scale model with those from the 1/10th-scale model for a position not likely to be seriously affected by the presence of the aircraft structure.

Antennas for the 1/10th-scale model were made using etched microstrip circuit-board techniques. The radiating elements were scaled directly from the full-sized elements. The feed lines were too narrow to scale, and therefore a modified feed circuit was designed and tested for use on the 1/10th-scale model. The elements were combined in a 1-by-8 array with appropriate phasing for the beam position being modeled.

The scale-model antennas were mounted on a 1/10th-scale ground plane using the same coordinates as the full-scale ground plane. Elevation and conical patterns were taken for comparison with full-scale patterns. A 1/10th-scale Convair 880 was used to model the aircraft. After installation of the antennas on the model, the previously recorded patterns were repeated.

Figure 6-7 compares the radiation patterns of the phased-array flight antenna with the 1/10th-scale model array for beam position 2. Since antenna efficiency cannot be scaled, no particular gain is implied in these patterns. Pattern shape is the only comparison that can be made.

TABLE 6-2. PHASED-ARRAY CIRCULAR FLIGHT SUMMARY

Date	Elevation angle, deg	Elevation beam position	Figure
Sep. 24, 1974	28	3	6-2
Oct. 29, 1974	16	2 and 3	6-3
Oct. 24, 1974	19	Not recorded	6-4
Nov. 21, 1974	19	5	6-5
Oct. 23, 1974	25	4	6-6

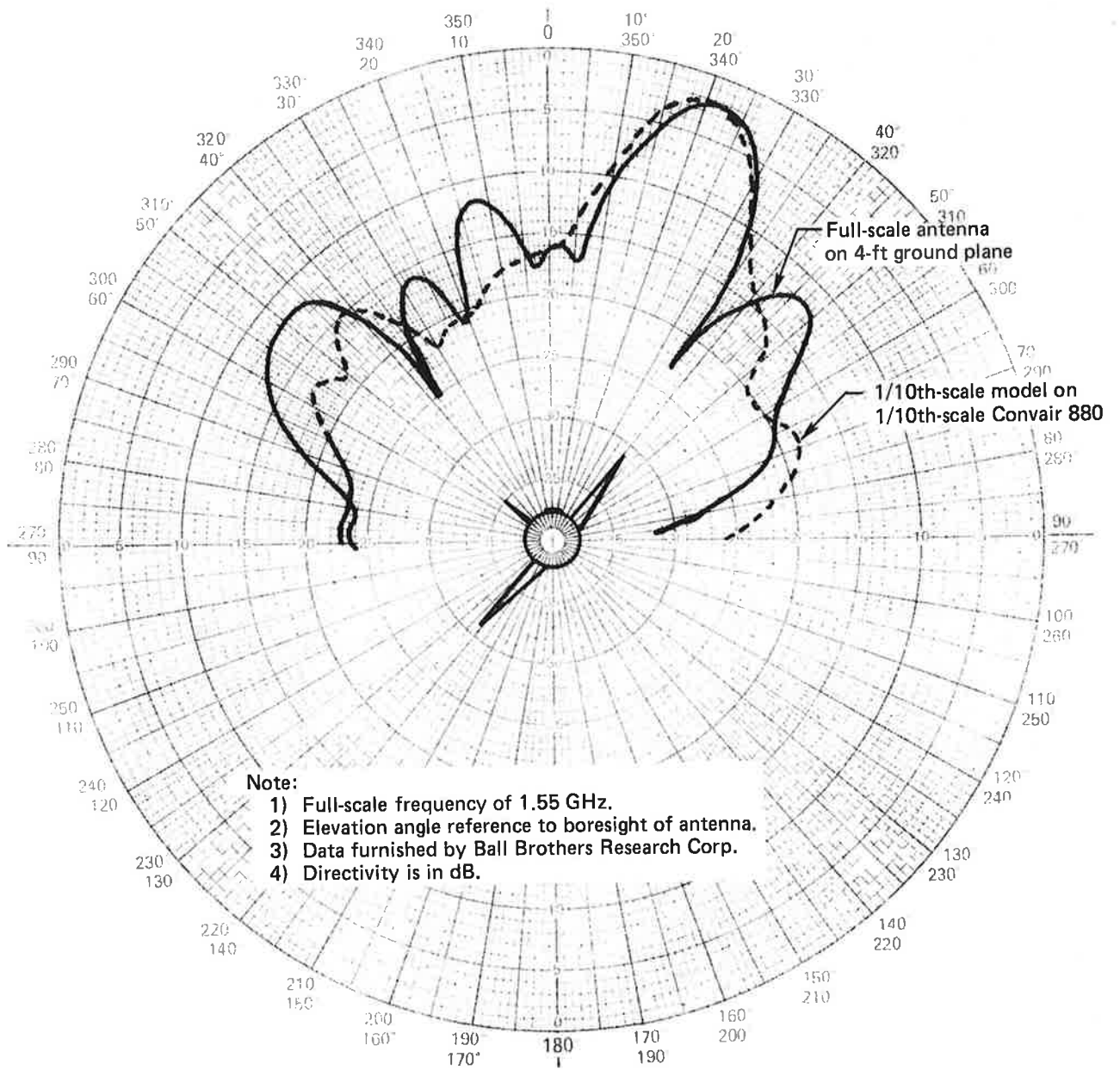


Figure 6-7. Phased-Array Roll-Plane Directivity Determined from Antenna Range Measurements, Beam Position 2

7. PATCH ANTENNA TEST RESULTS

Four circular-path tests were conducted with the patch antenna. Results are plotted in figures 7-1 through 7-4. A summary of the test conditions is tabulated in table 7-1.

TABLE 7-1. PATCH ANTENNA CIRCULAR FLIGHT SUMMARY

Date	Elevation angle, deg	Figure
Oct. 23, 1974	25	7-1
Nov. 21, 1974	19	7-2
Oct. 29, 1974	16	7-3
Oct. 24, 1974	19	7-4

From figures 7-1, 7-2, and 7-3, it is apparent that the patch antenna had a peak gain of approximately 4 dB forward over the nose at elevation angles above 15°. The gain gradually decreased as the satellite bearing angle changed toward the broadside and aft directions or as the satellite elevation angle reduced toward the horizon. Gain in the broadside and more aft directions was about 0 dB at an elevation angle of 16°, increasing to about 2.5 dB at a 25° elevation angle.

Gain data acquired during a ground test at NAFEC is given in table 7-2. This data shows that gain in the forward over-the-nose direction at a higher elevation angle was also on the order of 4 dB (3.7 dB measured), decreasing to about 2.5 dB aft of broadside. These results are consistent with the data of figures 7-1, 7-2, and 7-3.

**TABLE 7-2. PATCH ANTENNA GAIN DATA,^a JANUARY 21, 1975,
ELEVATION ANGLE = 40°**

ATS-6 direction, deg		C/N ₀ , dB-Hz		Received signal level, -dBW	Antenna gain, dB
Relative bearing	Elevation	Real-time measured	Computer analyzed		
0	40	47.5	N/A	151.6	3.7
16	40	47.5	N/A	151.6	3.4
164	40	45.9	N/A	153.2	2.3 ^b

^aData acquired during NAFEC ground test.

^bDirect gain calibration using quad helix was not available. ATS-6 downlink calibration measurements made at other times and locations during the same test have been used.

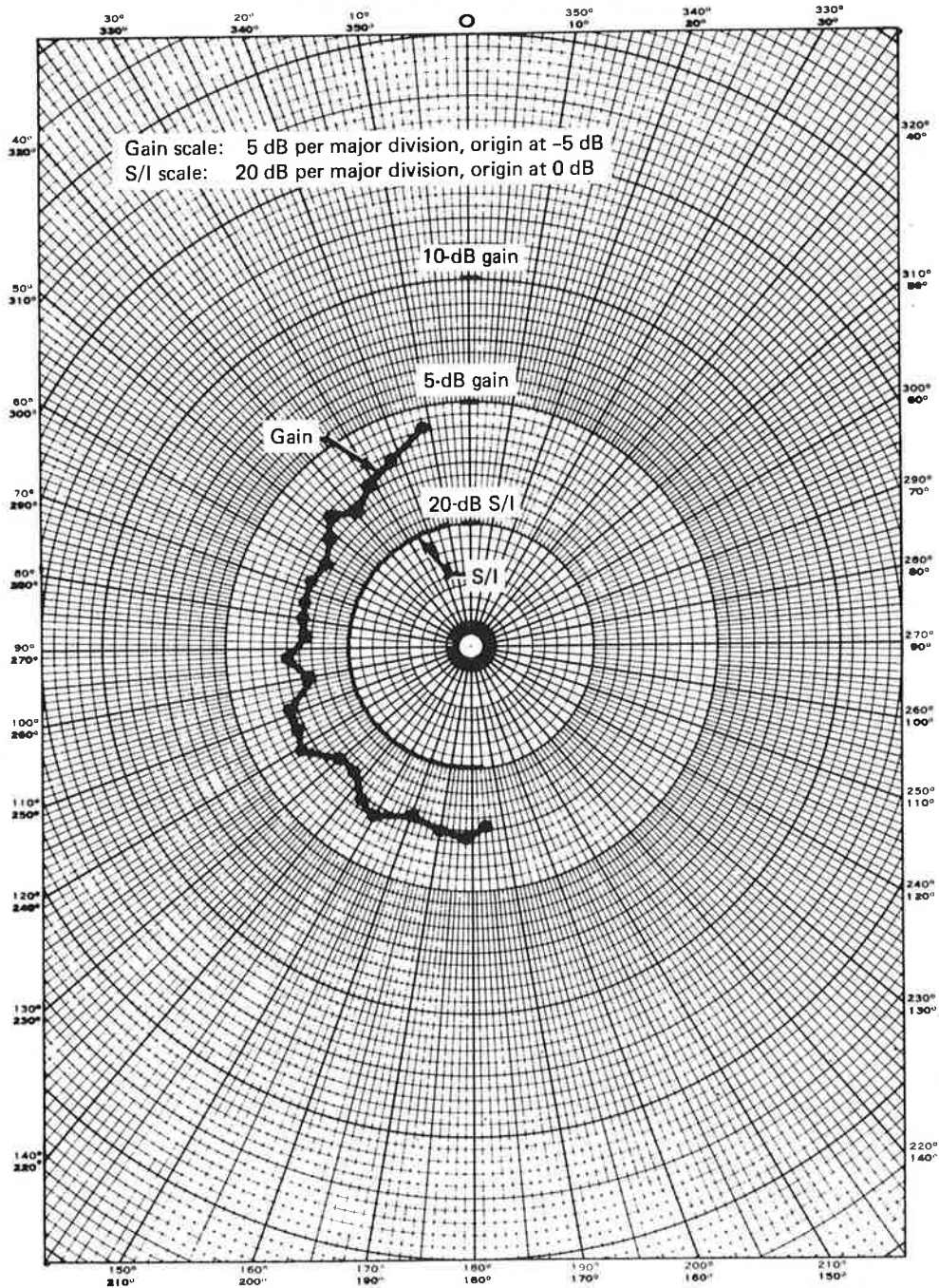


Figure 7-1. Patch Antenna Gain and S/I, October 23, 1974, Elevation Angle = 25°

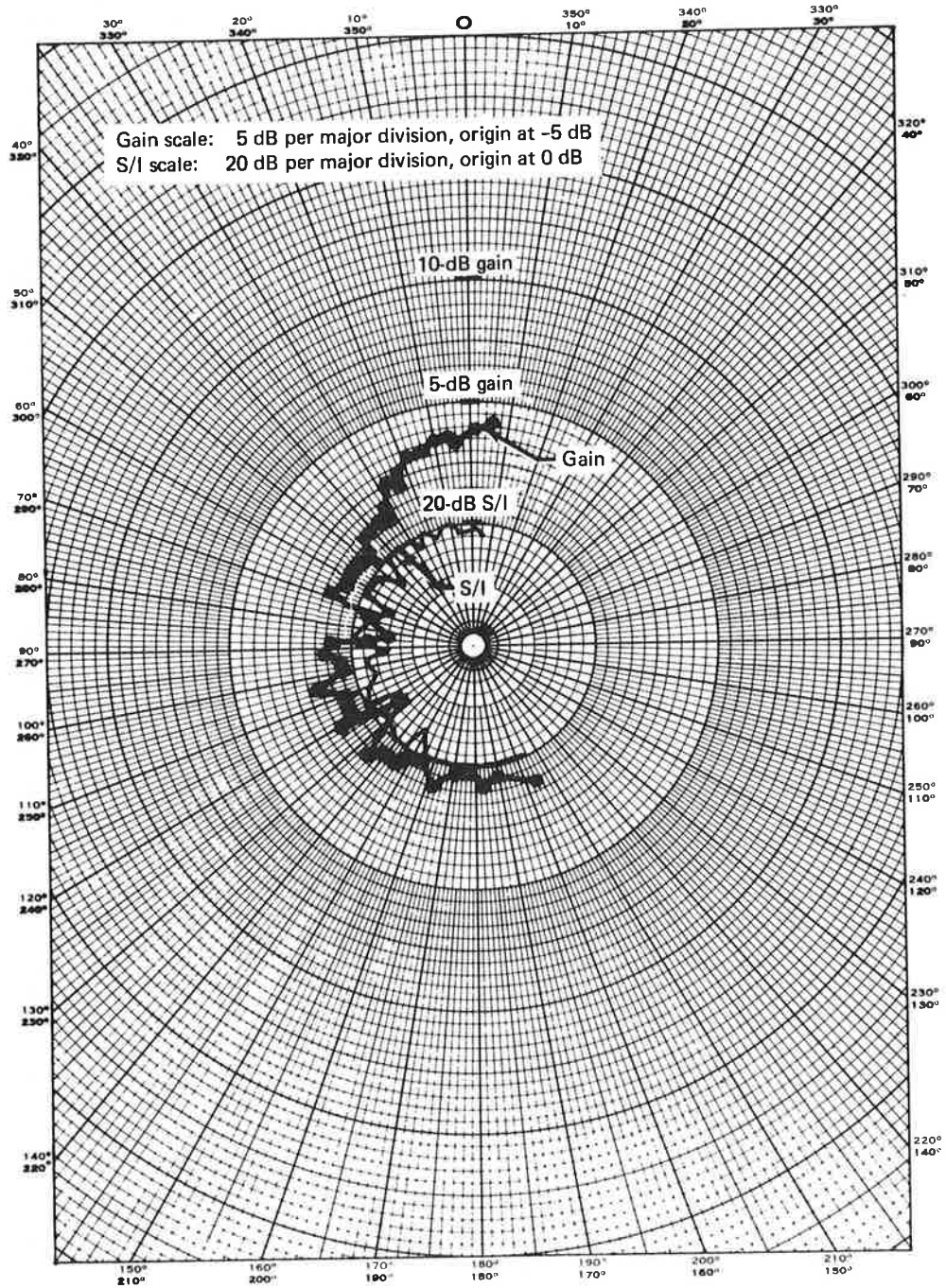


Figure 7-2. Patch Antenna Gain and S/I, November 21, 1974, Elevation Angle = 19°

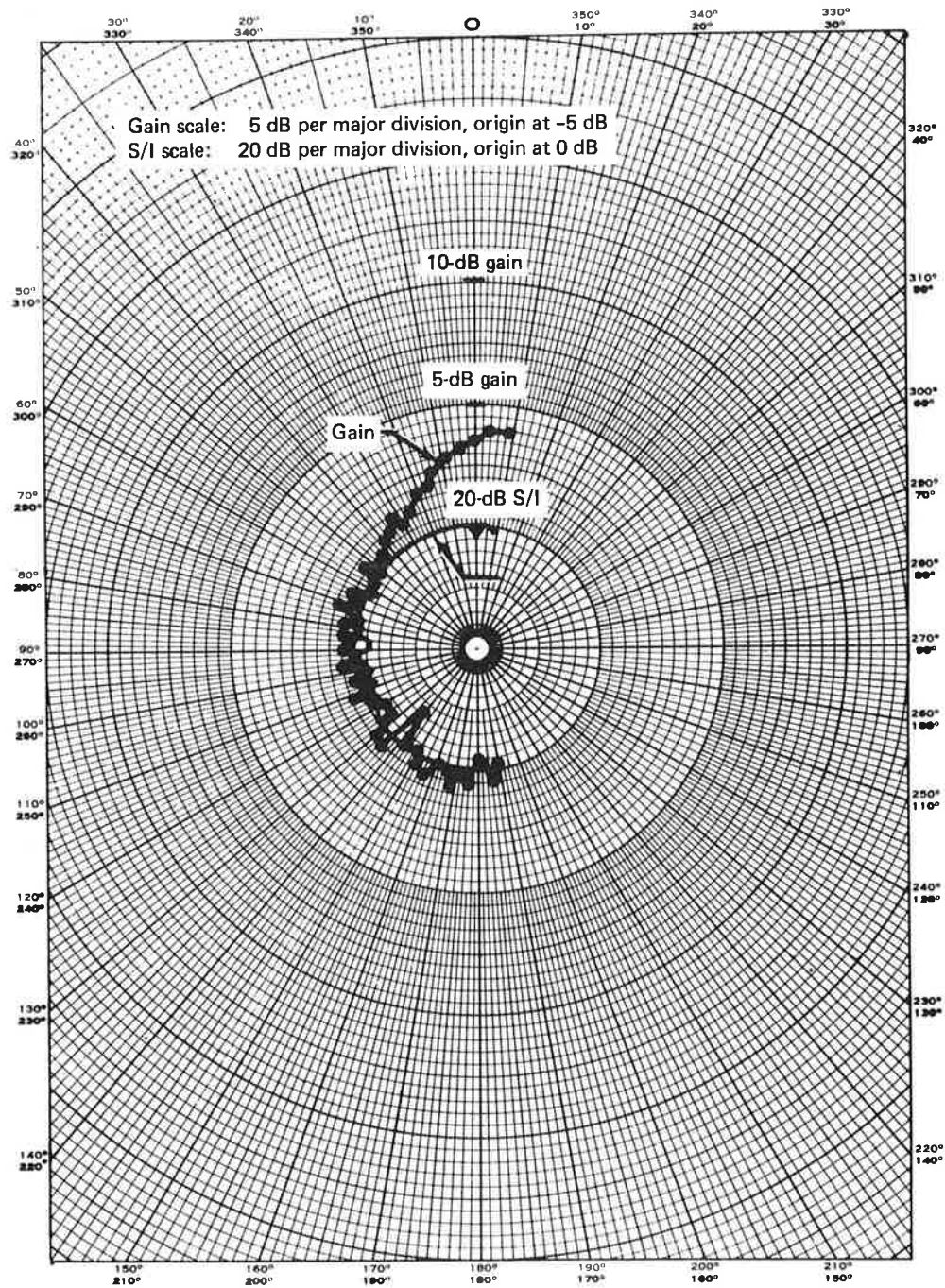


Figure 7-3. Patch Antenna Gain and S/I, October 29, 1974, Elevation Angle = 16°

Data presented in figure 7-4 for the October 24, 1974, test is somewhat anomalous. This test indicated a gain somewhat higher than expected in the forward direction and somewhat lower than expected in other directions for an elevation angle of 19° . The reason for these deviations from other data is not known. Antenna range data for this antenna is not available for inclusion in this report.

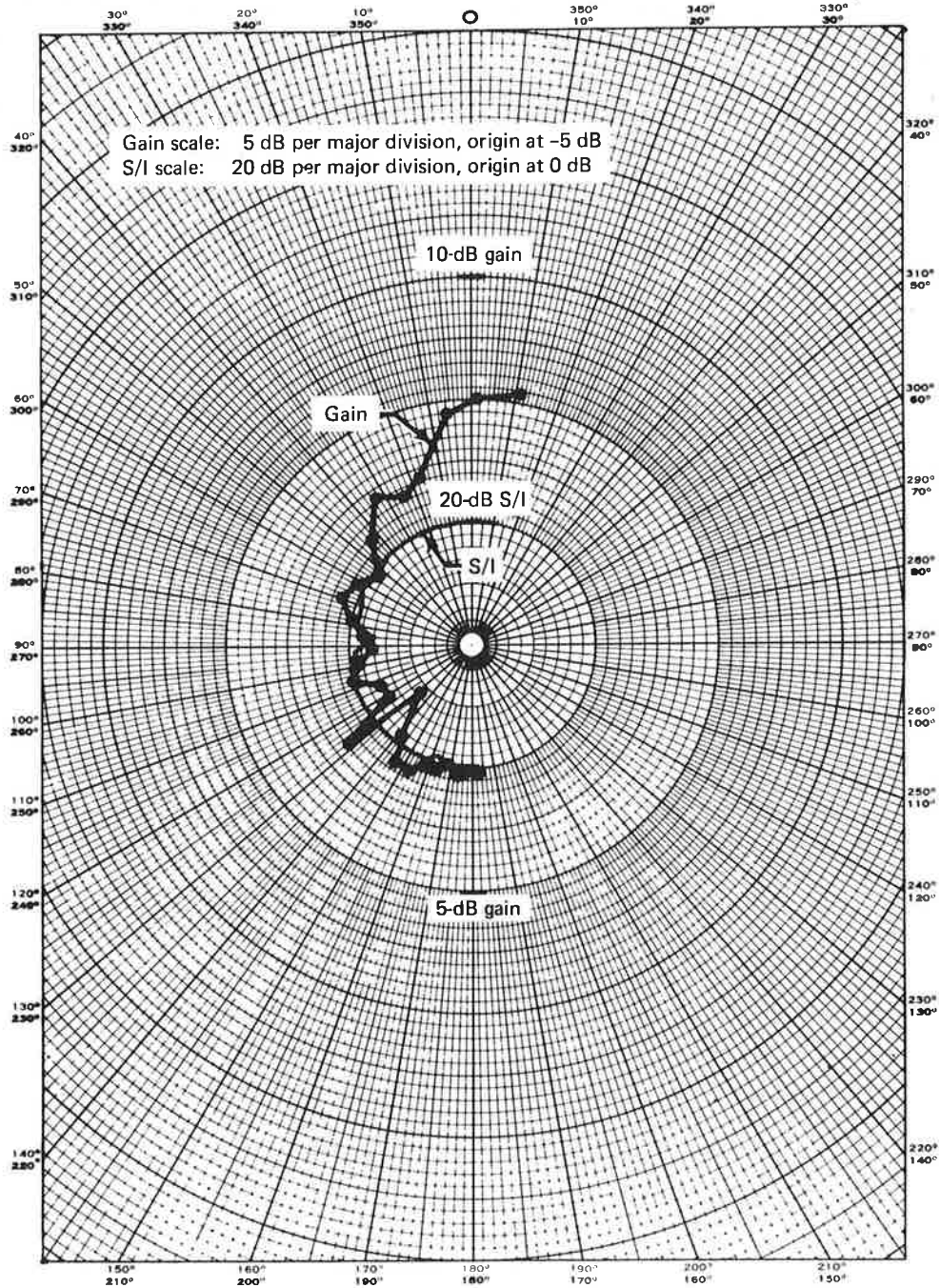


Figure 7-4. Patch Antenna Gain and S/I, October 24, 1974, Elevation Angle = 19°

REFERENCES

- 1-1 "Integrated Test Plan for ATS-F L-Band Experiment," NASA/GSFC report TP-750-73-1, September 1973.
- 3-1 "ATS-6 Multipath/Ranging/Digital Data L-Band Experimental Program, Phase I," report FAA-RD-73-57-1, contract FA69WA-2109, April 1973.
- 3-2 R. E. Munson, "Conformal Microstrip Antennas and Microstrip Phased Arrays," IEEE Trans. on Antennas and Propagation, January 1974, p. 74-78.
- 3-3 G. G. Sanford, "Conformal Microstrip Phased Array for Aircraft Tests with ATS-6," National Electronics Conference, Chicago, 1974, p. 252-257.
- 3-4 G. G. Sanford and L. Klein, "Development and Test of Conformal Microstrip Airborne Phased Array for Use with the ATS-6 Satellite," presented at IEE Conference on Antennas for Aircraft and Spacecraft, London, England, June 1975.
- 3-5 T. Olsson and B. P. Stapleton, "L-Band Orthogonal-Mode Crossed-Slot Antenna and VHF Crossed-Loop Antenna," contract DOT-TSC-130, August 1972.
- A-1 H. Staras, "Rough Surface Scattering on a Communication Link," Radio Science. vol. 3 (New Series), no. 6, 1968.

APPENDIX

PREDICTION OF S/I FROM ANTENNA RANGE DATA FOR SLOT-DIPOLE ANTENNAS

This appendix provides the mathematical basis for the estimation of expected S/I from antenna range data used in conjunction with an oceanic multipath scatter model.

The performance of avionics systems using RF links will in general be degraded both by noise and multipath interference. Hence, the multipath rejection characteristics of an operational aircraft antenna, as well as gain, need to be known and must meet appropriate criteria. Because of the high cost of aircraft operation and satellite test hours, it is impractical to field test all candidate operational antennas to measure multipath rejection characteristics. A means of predicting multipath performance based on a multipath propagation model and antenna characteristics as measured on an antenna range is therefore needed.

Using the closed-form "steepest descent" multipath characterization model (see ref. A-1), we determine the coupling between the sea return and the aircraft antenna by assuming that the complex polarization vector of the scattered signal is equal to the direct signal polarization vector as modified by the specular-point complex Fresnel reflection coefficients. The direct signal is taken to be a perfect right-hand circular vector.

Thus, we have:

$$\begin{aligned}(S/I)_{dB} &= S_{dB} - I_{dB} \\ S_{dB} &= 10 \log_{10} \{ |\overline{G}(\gamma, \phi) \cdot \overline{D}|^2 \} \\ I_{dB} &= \{ |\overline{G}(-\gamma, \phi) \cdot \overline{M}(\gamma)|^2 \} ,\end{aligned}$$

where \cdot denotes the inner product and:

- S = received direct signal
- I = received multipath signal
- $\overline{G}(\gamma, \phi)$ = complex aircraft antenna gain polarization vector
- \overline{D} = direct signal complex polarization vector (assumed to be 0 dB ellipticity RHC for all γ, ϕ)

- $\overline{M}(\gamma)$ = complex multipath polarization vector
 γ = elevation angle from aircraft to satellite
 ϕ = azimuth angle from aircraft to satellite measured relative to fuselage centerline

Vector $\overline{G}(\gamma, \phi)$ is determined from scale-model antenna range measurements. These measurements, taken every 2° in both azimuth and elevation, entail determination of the antenna gain for right- and left-hand circular polarization and for horizontal, vertical, and two other linear polarizations. Since the antenna polarization ellipse is defined by three quantities (major axis, minor axis, and skew angle), a minimum of three linear polarization measurements is required. The fourth linear polarization measurement is made to provide redundancy. The vectors \overline{D} and $\overline{M}(\gamma)$ have been derived from

$$\begin{aligned}\overline{D} &= \hat{x} + e^{j\pi/2}\hat{y} \\ \overline{M}(\gamma) &= R_H(\gamma)\hat{x} + R_V(\gamma)e^{j\pi/2}\hat{y},\end{aligned}$$

where:

\hat{x}, \hat{y} = unit vectors in the conventional directions used to define horizontal and vertical polarization

R_H = complex horizontal polarization reflection coefficient

R_V = complex vertical polarization reflection coefficient

Results of this analysis are given in figure 5-11, where S/I values are plotted for 2° increments in azimuth and elevation. Due to antenna system symmetry, results are given for one side only. The four linear polarization measurements required to characterize the antenna sufficiently for these calculations were not available for the top-mounted antenna. Therefore, only the side-mounted wing-root antenna has been included in the calculation of predicted S/I. In actuality, the top-mounted antenna, rather than the side antenna, would be used directly fore and aft. The S/I predictions for ϕ near 0° and 180° are therefore somewhat academic but are of interest for comparison with the experimental data.

A rigorous determination of the multipath interference requires integration of the complex antenna pattern over the total ocean surface. In the derivation described here, we have assumed the "steepest descent" solution and have characterized the multipath signal by its specular-point values. The results presented are thus not considered to be exact but are believed to be a good approximation, especially for modest sea-slope cases. In fact, the above approach may be argued to provide worst-case estimates of the antenna S/I parameter since the earth's divergence effect is neglected and the scattered energy is assumed to arrive only from the specular-point region. For grazing angles on the order of 10° , the divergence factor will attenuate the I component by approximately 2 dB and if

the aircraft antenna pattern had been integrated over the diffuse sea-scatter process, its well-known rolloff characteristics (θ -plane) would provide further multipath rejection. A small number of calculations employing integration over the total ocean surface have been performed. These results are presented in section 5.2. In all cases, the surface integration predicts a larger S/I value than the specular-point model described above. Because of the large computational effort, calculations using integration over the surface were made for only a few selected combinations of geometry and sea state.

U. S. DEPARTMENT OF TRANSPORTATION
TRANSPORTATION SYSTEMS CENTER
KENDALL SQUARE, CAMBRIDGE, MA. 02142
OFFICIAL BUSINESS
PENALTY FOR PRIVATE USE: \$300



POSTAGE AND FEES PAID
U. S. DEPARTMENT OF TRANSPORTATION

518